1 Modeling riverbed elevation and bedload tracer transport

resting times using Fractional Laplace motion

- 3 Zi $Wu^{1,2,3,4*}$ and Arvind Singh^{4,*}
- ¹State Key Laboratory of Hydroscience and Engineering, Tsinghua University, Beijing 100084,
- 5 China.
- ²Key Laboratory of Hydrosphere Sciences of the Ministry of Water Resources, Tsinghua
- 7 University, Beijing 100084, China.
- 8 ³Department of Hydraulic Engineering, Tsinghua University, Beijing 100084, China.
- ⁴Department of Civil, Environmental, and Construction Engineering, University of Central
- 10 Florida, Orlando, Florida, USA.
- *Corresponding authors: Zi Wu (<u>wuzi@tsinghua.edu.cn</u>) and Arvind Singh (<u>Arvind.Singh@ucf.edu</u>).

12 Key points:

- 13 > The Fractional Laplace motion (FLM) can be used to describe the evolution of the
- distribution of bed elevation increments over different timescales.
- ► Correctly predicting bed elevation fluctuations at the finest timescale is critical for estimating
- resting times for bedload tracer transport.
- FLM model provides a means of robustly estimating the tail exponent of the resting time
- distribution in case of insufficient data series length.

Abstract

19

20

21

22

23

24

25

26

27

28

29

30

31

32

33

34

35

36

37

38

Riverbed elevations play a crucial role in sediment transport and flow resistance, making it essential to understand and quantify their effects. This knowledge is vital for various fields, including river engineering and stream ecology. Previous observations have revealed that fluctuations in the bed surface can exhibit both multifractal and monofractal behaviors. Specifically, the probability distribution function (PDF) of elevation increments may transition from Laplace (two-sided exponential) to Gaussian with increasing scales, or consistently remain Gaussian, respectively. These differences at the finest timescale lead to distinct patterns of bedload particle exchange with the bed surface, thereby influencing particle resting times and streamwise transport. In this paper, we utilize the fractional Laplace motion (FLM) model to analyze riverbed elevation series, demonstrating its capability to capture both mono- and multifractal behaviors. Our focus is on studying the resting time distribution of bedload particles during downstream transport, with the FLM model primarily parameterized based on the Laplace distribution of increments PDF at the finest timescale. Resting times are extracted from the bed elevation series by identifying pairs of adjacent deposition and entrainment events at the same elevation. We demonstrate that in cases of insufficient data series length, the FLM model robustly estimates the tail exponent of the resting time distribution. Notably, the tail of the exceedance probability distribution of resting times is much heavier for experimental measurements displaying Laplace increments PDF at the finest scale, compared to previous studies observing Gaussian PDF for bed elevation.

Plain Language Summary

39

40

41

42

43

44

45

46

47

48

49

50

51

52

53

54

55

56

The evolution of riverbed elevations is difficult to describe due to its highly variable and strongly non-linear nature. Understanding and quantifying dynamics of riverbed elevations are important for river engineering and stream ecology, and serve as the basis for numerical models of predicting sediment transport as well as interpreting stratigraphy from the past records. Through laboratory experiments, we have observed that the form of elevation increments PDF can change from Laplace to Gaussian as the timescale increases. This phenomenon is successfully modeled in this paper for the first time by the fractional Laplace motion, which essentially generates bed elevation series for the evolution of bed surface height at a certain spatial location of the bed. This series contain information on how long a bedload particle can rest (resting time) in the riverbed before it can be re-entrained to move downstream, the determination of which by other means (e.g. particle-tracking measurements) is challenging. By extracting resting times embedded in this bed elevation series, we obtain statistics (i.e. the tail behavior of the resting time distribution) that are key for correctly modeling the transport of bedload particles, and more specifically, that can help us to understand the anomalous bedload diffusion process.

Key Words: Fractional Laplace motion, bed elevation, bedload transport, resting time distribution, anomalous diffusion

1. Introduction

57

58

59

60

61

62

63

64

65

66

67

68

69

70

71

72

73

74

75

76

77

78

79

The evolution of riverbed elevations is difficult to describe as it exhibits high variability due to formation and migration of bedforms across multiple scales and types, fluctuations in grain size distribution, and the complex non-linear response to alterations in stream hydrology, among other influential variables. Understanding and quantifying dynamics of riverbed elevations are important for river engineering, stream ecology and can provide morphological boundary conditions to numerical models for predicting the transport of sediments, contaminants, microorganisms, as well as interpreting stratigraphy from the past records (Aberle et al., 2010; Best, 2005; Coleman & Melville, 1994; Ganti et al., 2014; Guala et al., 2014; Jerolmack & Mohrig, 2005; Jiang et al., 2022; Lee et al., 2022; Li et al., 2023; McElroy & Mohrig, 2009; Nikora & Walsh, 2004; Nikora et al., 1997; Simons & Richardson, 1962; Singh et al., 2023; Singh et al., 2009; Singh et al., 2013; Strom et al., 2004; Wu & Chen, 2014; Yarnell et al., 2006; Zhan et al., 2024; Zhang et al., 2024). Several studies have focused on characterizing riverbed elevations using different approaches of numerical simulations (e.g. Khosronejad & Sotiropoulos, 2017; Sotiropoulos & Khosronejad, 2016; Viparelli et al., 2010), experiments (e.g. Aberle & Nikora, 2006; Monsalve et al., 2017; Pender et al., 2001; Singh et al., 2011; Wong & Parker, 2006; Wong et al., 2007), and field observations (e.g. Haschenburger, 1999, 2006; Hassan & Church, 1994; Nikora & Walsh, 2004; Parsons et al., 2005; Vázquez-Tarrío et al., 2021). For example, Pender et al. (2001) observed that for the spatial bed elevation, the probability distribution function (PDF) of bed elevation fluctuations around the mean shows Gaussian shape for well sorted sediments. Wong et al. (2007) analyzed temporal bed elevation data from the plane-bed of uniform grain size distribution and suggested that the bed elevation fluctuations around the mean can be

81

82

83

84

85

86

87

88

89

90

91

92

93

94

95

96

97

98

99

100

101

102

approximated using Gaussian distribution. However, they observed a slight deviation in the tails of the PDFs for extreme fluctuations. Aberle & Nikora (2006) explored the bed elevations PDF for armored bed conditions and argued that with increasing armoring discharge the range of bed elevation increases whereas its probability around the zero mean decreases. For field observations at the flood event scale, elevation data for the gravel-bed rivers suggest that the distribution of scour and fill depths during floods, which are similar to the elevation increments as measured in previous studies, follows an exponential distribution (Haschenburger, 1999, 2006; Hassan & Church, 1994; Vázquez-Tarrío et al., 2021). In studying the streamwise transport of bedload sediment particles, the information embedded in the riverbed elevation fluctuations is particularly useful (Viparelli et al., 2022). Since the pioneering work of Einstein (Einstein, 1937; Einstein, 1950), the bedload particle transport has been theoretically described by two alternating processes of the particle hop (or step, the successive motions of a particle from start to stop) and particle rest (the static period between two hops, the duration of which is termed as the resting time). Recent investigations on the anomalous behaviors of streamwise transport of tracer particles have mostly attributed the source

pioneering work of Einstein (Einstein, 1937; Einstein, 1950), the bedload particle transport has been theoretically described by two alternating processes of the particle hop (or step, the successive motions of a particle from start to stop) and particle rest (the static period between two hops, the duration of which is termed as the resting time). Recent investigations on the anomalous behaviors of streamwise transport of tracer particles have mostly attributed the source of this phenomenon to the heavy-tailed distribution of resting times (Bradley, 2017; Hassan et al., 2013; Martin et al., 2012; Pelosi et al., 2016; Pierce & Hassan, 2020a; Wu et al., 2020; Wu et al., 2019a; Wu et al., 2019b). Under this context, the behavior of riverbed elevation fluctuations characterizing the critical events of sediment particle deposition (related to upward motion of bed surface) and entrainment (downward surface motion) has provided a compact format of information, based on which the extraction of representative resting times of particles is possible (Martin et al., 2014; Pierce & Hassan, 2020b; Voepel et al., 2013). Specifically, focusing on one single particle, its deposition on the riverbed surface on a certain level causes the increase of the

elevation. Then after some time when the same particle is remobilized (entrained), the surface elevation decreases beneath that particular level due to the scour and the time difference between the two adjacent events by definition is an instance of the resting time of a particle.

103

104

105

106

107

108

109

110

111

112

113

114

115

116

117

118

119

120

121

122

123

124

125

To the best of our knowledge, Voepel et al. (2013) are the first who proposed the method of extracting resting times through empirical time series of riverbed elevation fluctuations. This method essentially offers an alternative to the conventional means of measuring resting times by tracking trajectories of bedload particles from a Lagrangian perspective. Consequently, it simplifies the otherwise complicated experimental setup to recording elevations of the riverbed surface at fixed streamwise positions, which is inherently Eulerian. Several different models had been proposed for the purpose of generating riverbed surface elevation time series ever since (Martin et al., 2014; Pierce & Hassan, 2020b), which were then used for characterizing tails of the resting time distribution aiming at studying the downstream anomalous transport of bedload tracer particles. However, the obtained elevation time series, either experimentally (Martin et al., 2014) or numerically (Martin et al., 2014; Pierce & Hassan, 2020b), exhibited monofractal behavior, that is, the increments PDF of the series is consistently Gaussian across different timescales. As a comparison, there had been different experimental investigations during which multifractal behaviors for the bed surface elevation series were observed (Aberle & Nikora, 2006; Nikora & Walsh, 2004; Singh et al., 2011; Singh et al., 2012b), revealing that at the finest timescale (the sampling interval) the increments PDF is Laplace-like while at some larger timescale it is Gaussian. Given its key role in characterizing the events of deposition and entrainment of particles, the different form of increments PDF at the finest timescale is critical in affecting the tail characteristics of the resting time distribution, thereby further influencing the streamwise bedload particle transport.

In fact, the gradual transition of increments PDF (of the time series) from Laplace to Gaussian as the timescale increases had also been observed and studied in other processes like that for hydraulic conductivity (Meerschaert et al., 2004) and sediment transport rates (Ganti et al., 2009), for example, which resulted in the development and application of a novel approach as the subordinated fractional Brownian motion (Meerschaert et al., 2004). This model is also known as the fractional Laplace motion (FLM) because at some fine scale the increments have a Laplace distribution (Kozubowski et al., 2006). As a brief introduction, Laplace motion is a stochastic process whose increments at some scale a show a symmetric two-sided exponential distribution (with respect to the mean at x = 0), which is also known as the Laplace distribution with its PDF expressed as:

$$f(x) = \frac{1}{\sqrt{2}\sigma} e^{-\frac{\sqrt{2}}{\sigma}|x|},\tag{1}$$

where σ is the standard deviation of the Laplace distribution (Ganti et al., 2009; Meerschaert et al., 2004). Laplace motion is a special case (with Hurst exponent H = 0.5) of fractional Laplace motion (Kozubowski et al., 2006), which can be generated based on a fractional Brownian motion (fBM) process $B_H(\cdot)$, whose operational time does not follow a physical time but is given instead by a Gamma process Γ_t with stochasticity:

$$L(t) = B_H(\Gamma_t), \tag{2}$$

143 where the Hurst exponent H can be in the range of (0, 1). Note that fBM exhibits a correlation 144 function defined as

145
$$E[B_{H}(t)B_{H}(s)] = \frac{1}{2}(|t|^{2H} + |s|^{2H} - |t - s|^{2H}),$$
 (3)

147

148

149

150

151

153

154

155

156

157

158

159

160

161

162

163

164

165

166

167

where E(.) represents the expectation operator (Ganti et al., 2009). When H = 0.5, $B_H(t)$ reduces to the standard Brownian motion with independent increments, however, for other values within the range of 0 < H < 1, the increments of $B_H(t)$ demonstrate positive correlation for H > 0.5 and negative correlation for H < 0.5.

The increments of the Gamma process $(\Gamma_{t+v} - \Gamma_t)$ have a Gamma distribution with the shape parameter v and the scale parameter as unity, and its PDF can be expressed as:

$$g(x) = \frac{1}{\Gamma(\nu)} x^{\nu - 1} e^{-x}.$$
 (4)

Equation (2) is also known as the subordinated stochastic process (Ganti et al., 2009), with the fBM $B_H(\cdot)$ called the parent process. For a specific process, two parameters—H (Hurst exponent) and σ (standard deviation)—are required for the parent process, along with one parameter ν (shape parameter) for the operational time. More discussions on the properties of the FLM by Eq. (2) and its parameters can be found in literature (Ganti et al., 2009; Kozubowski et al., 2006). In this paper, we apply the FLM model to describe fluctuations of riverbed elevation, aiming to reproduce its multifractal behaviors, particularly focusing on the Laplace distribution of the increments at the finest timescale. These distributions are then utilized for extracting resting times and analyzing the tail characteristics of the corresponding exceedance probability distribution. The paper is structured as follows. In the following section, we first briefly introduce the experimental data from field-scale laboratory experiments conducted at the St. Anthony Falls Laboratory, which is followed by details of the FLM model, as well as the algorithm used for extracting resting times. Section 3 starts with discussions on effects of parameters on the simulated shapes of increments PDF generated by the FLM model, and provides a demonstration of parameter estimation based on the empirical data. Also explored are

the conditions under which the FLM is reduced to a monofractal model, and how the size of dataset affects the numerical simulation results, as well as their implications. Summary and concluding remarks are provided in section 4.

The data used in this study are from the physical experiments conducted in the large

2. Data and methods

168

169

170

171

172

173

174

175

176

177

178

179

180

181

182

183

184

185

186

187

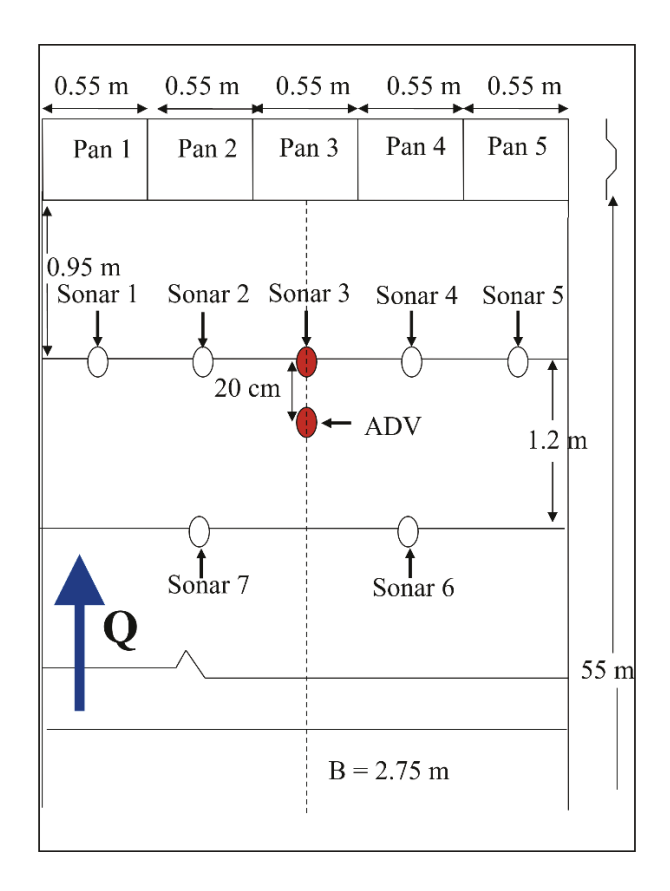
188

189

2.1. Experimental data for bed elevations

experimental flume at the St. Anthony Falls Laboratory, University of Minnesota. The flume was 85 m long, 2.75 m wide, and 1.8 m deep with a maximum discharge capacity of 8500 L/s. A 55 m long upstream section of the flume was used for this study. The flume is a partially sediment recirculating channel (Parker & Wilcock, 1993) while the water flows through the channel without recirculation. Intake of the water in the channel is directly from the Mississippi River. To ensure quasi-dynamic equilibrium in both water and bed surface transport, a constant water discharge (O) was introduced into the channel prior to data collection. The dynamic equilibrium state was assessed by verifying the stability of the 60-minute average total sediment flux (s(t)) at the downstream end of the test section. The data collected included time series of bed elevation, local velocity fluctuations using acoustic Doppler velocimetry (ADV), and instantaneous sediment transport rates s(t) using weighing pans at the downstream end of the 55 m long channel test section (see Figure 1), along with surface grain size distribution (Singh et al., 2010; Singh et al., 2012a; Singh et al., 2012b; Singh et al., 2009). Prior to the experimental run initiation, the channel bed consisted of a mixture of gravel and sand with overall median grain size $D_{50} = 7.7$ mm, $D_{16} = 2.2$ mm and D_{84} = 21.2 mm. The temporal bed elevations were measured using seven stationary submersible

sonar transducers of 2.5 cm diameter with a pinging frequency of 2.5 MHz, mounted at the end of rigid 1.5 cm diameter steel tubes. The transducers were placed approximately 0.3 m above the mean bed elevation and 1.2 m upstream of sediment flux measurement system. Bed elevations data were collected at intervals of 5 sec with a vertical precision of ~ 1 mm. These measurements were taken at the discharges of 2000 L/s and 2800 L/s corresponding to dimensionless Shield stresses of 0.058 and 0.099, respectively. For further information on the experiments, please refer to Singh et al. (2009 a, b, 2010, 2011, and 2012) and Ranjbar & Singh (2020). We acknowledge that the sampling interval, or temporal resolution, will have an effect on the identification of entrainment and deposition events. Events occurring within the 5-second interval will not be captured since there is no recorded information on the elevation of the bed surface at that specific position.



204

205

206

207

208

209

210

211

212

213

214

215

216

217

218

219

220

221

222

223

224

Figure 2 shows the time series of bed elevation (a, b) for the discharges of 2000 L/s and 2800 L/s, respectively, with their increments (c, d). As can be seen from the time series of bed elevation increments, several extreme fluctuations (spikes observed in c and d), resulting from the steep faces of bedforms (which were mainly dunes) in the elevation series are present, and the number of these fluctuations increases as the discharge increases for the same length of time series. This is due to faster movement of bed forms at higher discharges. For example, the average timescale for the movement of average-size bedform at the discharge of 2000 L/s is about 22 minutes, and 15 minutes for the discharge of 2800 L/s (for bedform (e.g. bedform height) characterization, see (Singh et al., 2012b)). These observed extreme fluctuations manifest themselves in the tails of the PDFs and can be seen in Figure 3(a) for the discharges of 2000 and 2800 L/s at the finest resolution of a = 1, corresponding to 5 sec. Here, a represents the ratio between the down-sampling time interval and the acquisition time interval. The PDFs of the bed elevation increments for both discharges at the time scale of 500 sec (a = 100) are shown in Figure 3(b). By Figure 3, we demonstrate that the PDF of bed elevation changes shape (from two-sided exponential, or Laplace, to Gaussian) as a function of scale a, suggesting multifractal behavior (Parisi & Frisch, 1985; Venugopal et al., 2006). The previous monofractal results have shown a Gaussian distribution for the elevation increments at the finest scale, whereas for the multifractal behavior, it is a Laplace distribution at the finest scale. This distinction underscores the need for a model capable of capturing the correct process at the finest scale, which directly contributes to an appropriate description of the resting time distribution, and consequently, to the streamwise transport of bedload particles.

We note that in a prior study conducted by Singh et al. (2012), the analysis of the identical experimental dataset revealed that the tails of the elevation increments PDF exhibited a decay consistent with a power-law distribution. However, our current investigation focuses on characterizing the central portion (body) of the increments PDF, which we find to resemble a Laplace distribution, particularly evident at the finest timescale (see Figure 3a). This major difference in analysis stems from the specific aim of our paper, which centers on examining the distribution of resting times for bedload particle transport. Our emphasis lies in scrutinizing the body of the increments PDF, which unveils subtle fluctuations in the bed surface, offering insights into the dynamics of particle deposition and entrainment events.

Although extreme events of scour and deposition are represented by tails of the increments PDF, they may not be directly responsible for extreme values of resting times, which are more dependent on the sequence of single events (e.g. successive negative increments may scour a remarkable depth to entrain buried particles) instead of their magnitudes. On the other hand, these extreme events of scour and deposition may also be constrained by the lower boundary of the riverbed (such as the bed rock at limited depth), implying that the increments PDF cannot maintain the power-law decaying in its tails (which motivates the use of the truncated Pareto distribution for the tails of increments PDF as in Singh et al. (2012b)). That said, we emphasize that it remains unclear whether the above-mentioned differences regarding power-law and exponential tails for bed elevation increments PDF will play an important role in affecting the tail behavior of resting time distributions, which is crucial to characterize the anomalous bedload transport, and will be investigated through obtaining the resting times from the elevation time series in this paper.

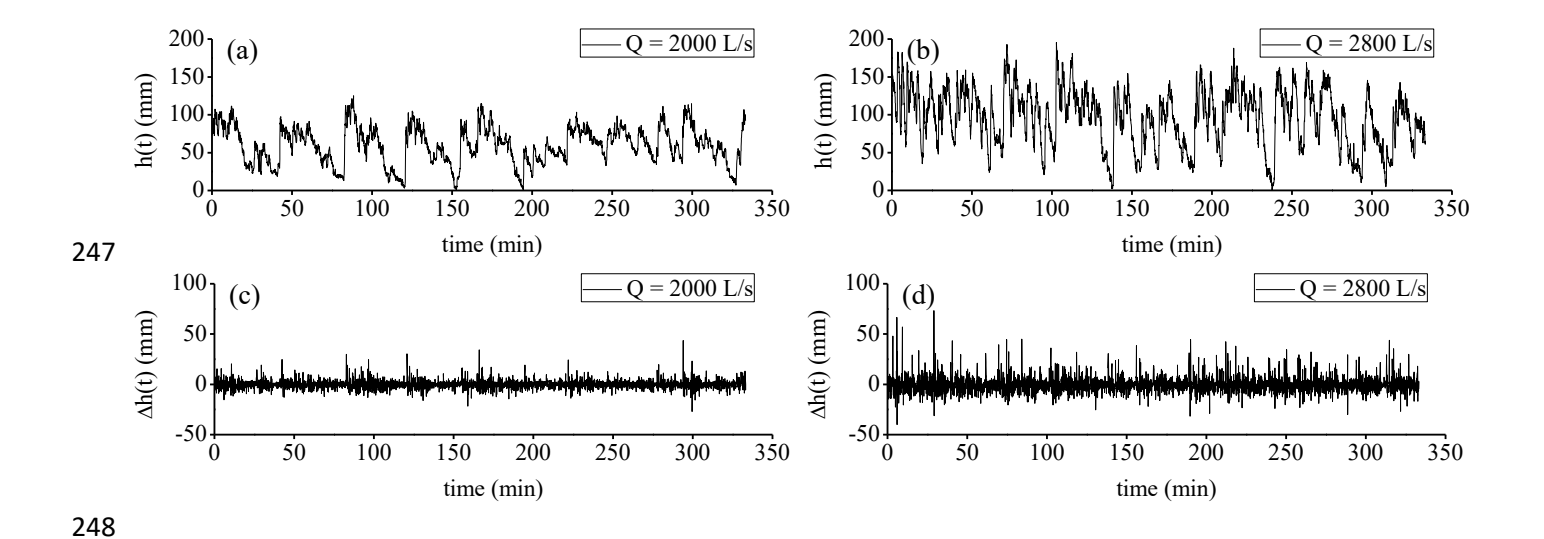


Figure 2: Time series of bed elevations h(t) (a, b), and their increments computed as $\Delta h(t) = h(t + a) - h(t)$ for the discharges of 2000 L/s and 2800 L/s, respectively (c, d), collected at the downstream end and in the centerline of the channel at sonar 3 (see Singh et al. 2010, for schematic). The increments shown in (c) and (d) were computed at the finest resolution, a = 1, corresponding to the sampling interval of bed elevation, $\Delta t = 5$ sec. As can be seen the bedforms are present at both discharges and the variability increases with increasing discharge.

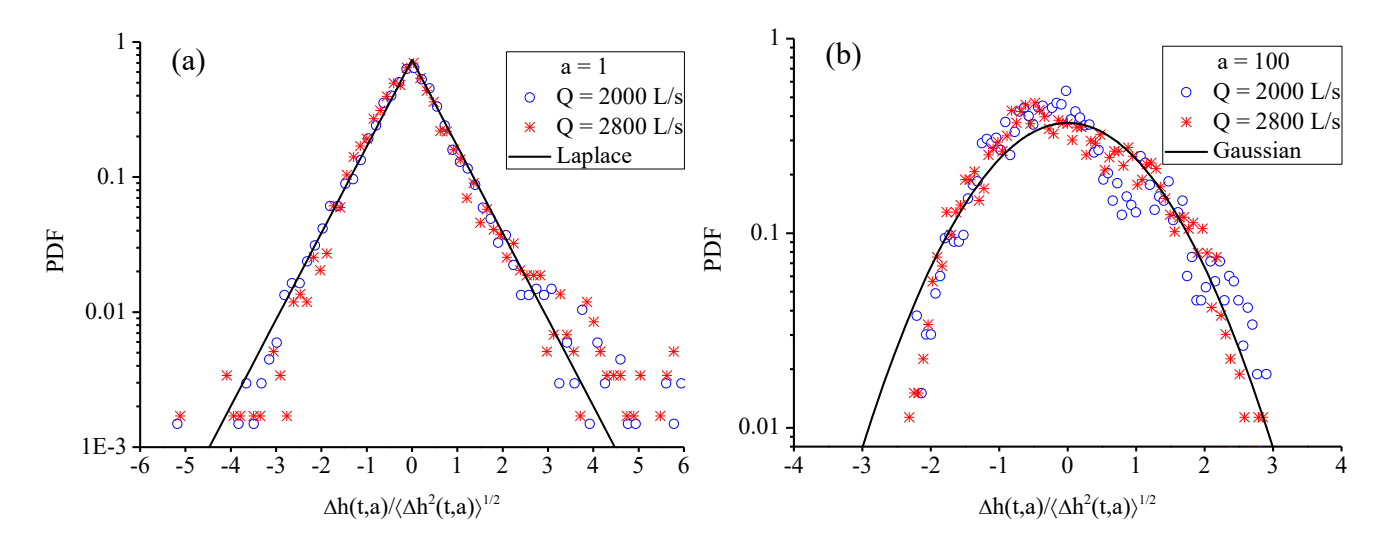


Figure 3: PDFs of increments of bed elevations at the discharges of 2000 L/s and 2800 L/s for two different scales. The smaller scale (a) represents the finest resolution at which the bed elevations were sampled whereas the larger scale (b) represents approximately the timescale for larger bedforms. The solid black lines represent Laplace (symmetric two-sided exponential) distribution and Gaussian distribution in (a) and (b), respectively.

2.2. Resting times and bed surface elevations for bedload sediment transport

If we track a bedload sediment particle (tracer) during the transport, its streamwise behavior can be described by a series of steps (or hops, successive motions of the particle from the start to the end of the movement) punctuated by resting times of random durations, as sketched by Figure 4 (a). In the pioneering work of Einstein (1937), the two fundamental elements of step length and resting period are considered as random variables, introducing the probabilistic description for the bedload sediment transport. It has been shown that according to Einstein's theory and its later extension, the mean and variance for the PDFs of these two variables determine an advection-diffusion process (i.e. the coefficients of v and D_d) for the bedload transport:

$$\frac{\partial C}{\partial t} + c \frac{\partial C}{\partial x} = D_d \frac{\partial^2 C}{\partial x^2},\tag{5}$$

where C is the tracer concentration, t is time, c is the virtual velocity of the tracer plume, x is the streamwise coordinate, and D_d is the diffusion coefficient. However, recent studies have revealed anomalous diffusion of bedload tracers indicating faster (super-diffusion) or slower (sub-diffusion) scattering of the tracer plume for the asymptotic transport regime, which can be theoretically expressed, for example, based on the fractional advection-diffusion equation (e.g. see Schumer et al. (2009) and references therein):

$$\frac{\partial^{\gamma} C}{\partial t^{\gamma}} + c \frac{\partial C}{\partial x} = D_d \frac{\partial^{\alpha} C}{\partial x^{\alpha}}, \tag{6}$$

where $\gamma \neq 1$ and/or $\alpha \neq 2$ indicates anomalous diffusion, and the index γ can be specifically determined by the tail characteristics of the resting time PDF.

280

281

282

283

284

285

286

287

288

289

290

291

292

293

294

295

296

297

298

299

300

Compared with the relatively easy measurements and rich datasets existing for steps (step lengths) (Wu et al., 2023; Wu et al., 2021), the measurements for resting periods are much more difficult. The definition of resting times is essentially Lagrangian which has posed great difficulties in experimentally measuring the resting of a particle between two successive hops (or steps) by tracing along its trajectory, given that a single resting can be unexpectedly long when it gets buried after stopped traveling on top of the riverbed. This is particularly so in studying the anomalous diffusion of bedload tracer particles, because the tail of the resting time distributions is associated with extreme cases of long-time resting of particles, which plays a crucial role in determining the asymptotic diffusion regimes during bedload transport. Thus particle-tracking experiments in directly capturing resting times of bedload particles can hardly be insightful regarding demarcation of the tail characteristics of the resting time distribution, since both temporal and spatial scales of such experiments are usually small in laboratory (Liu et al., 2019). Conversely, the empirical method of determining the resting times based on the time series of riverbed elevations (Martin et al., 2014; Voepel et al., 2013) is Eulerian, translating measurements of an ensemble of resting times with respect to the transport of a single particle into that collected at a fixed streamwise position regarding the ensemble of different particles. This method enables a rapid capturing of a large number of resting times within a relatively short period of laboratory observations. For field cases, the riverbed elevation, for example, has been studied at the flood event scale using scour chains and scour indicators, providing information on scour and fill depths which are similar to the bed elevation fluctuations as measured in flume experiments, and can be seen as the variation of bed surface elevation at some coarser scale (Haschenburger, 1999, 2006; Hassan & Church, 1994; Vázquez-Tarrío et al., 2021).

In this paper, we follow intrinsically the same empirical method proposed by Voepel et al. (2013). Putting aside the specific definition on the unconditional exceedance distribution of resting times (Martin et al., 2014; Pierce & Hassan, 2020b; Voepel et al., 2013), the essence of this method is to extract all the resting times embedded in the bed elevation series, which is then considered as the ensemble (of resting times) for further analysis. The key for such an extraction is to identify a pair of adjacent deposition (bed surface increases across a certain elevation) and entrainment (after a period the bed surface decreases across the same elevation) events, the time difference between which gives an instance of the resting time.

In Figure 4 we qualitatively illustrate the relation between resting times and bed surface elevations for bedload sediment transport. For a specific resting period (e.g., as shown in Figure 4 b), the starting of it corresponds to the deposition of the tracer, leading to the increase in the bed surface elevation at a given spatial location A. The continued increase of the bed surface elevation indicates deposition of other particles at this same location (i.e. vertically above the tracer), while the decrease of the elevation means entrainment of this tracer, thus indicates the end of this considered resting period (Figure 4 b). An instance of resting time is thus extracted from the series of the bed surface elevations.

We need to emphasize that the transport of bedload particles studied in this paper follows the pattern described in Figure 4(a). Specifically, the bedload tracer particles considered (e.g., gravels or pebbles) move discontinuously, with most of the time spent stationary on the riverbed surface. Consequently, for a specific location on the surface, increases in elevation are solely attributable to the arrival and subsequent settling of particles, while decreases are associated with particle remobilization from the bed surface. This contrasts with situations involving the continuous motion of bed material, such as sheet flow. We also note that since multiple resting

times can be extracted from the series in Figure 4(b), we do not set a threshold for the bed elevation. Instead, we base the extraction on the variation of elevation at each time step of the measurement (as described in our algorithm at the end of this section). The elevation change during a time step can be substantial, as illustrated in Figure 2, in which case the deposition or entrainment events involve more than one particle. However, if multiple particles move and stop together, they share the same resting time.

An observation of Figure 2 suggests that, the negative increments (negative Δh) generally exhibit lower magnitudes compared to positive increments, indicating a higher (virtual) resolution in capturing the entrainment events. This higher resolution determines the resolution of the resulting resting times according to our algorithm devised based on the conceptual framework of Voepel et al. (2013). Although it is still possible that the negative increments may exceed the size of the largest particle, resulting in multiple particles sharing the same resting time, it is the best approach we can take to treat these samples as having only one resting time for statistical analysis at this specific temporal resolution of 5 seconds.

For the obtained PDF of resting times, the tail instead of the body of the PDF is significant, particularly in explaining the anomalous diffusion of bedload tracer transport. The extreme events of long resting times correspond to those particles buried deep and entrained later. It is observed from the elevation series that entrainments at deep locations are generally gentle, reflecting higher resolution in those measurements.

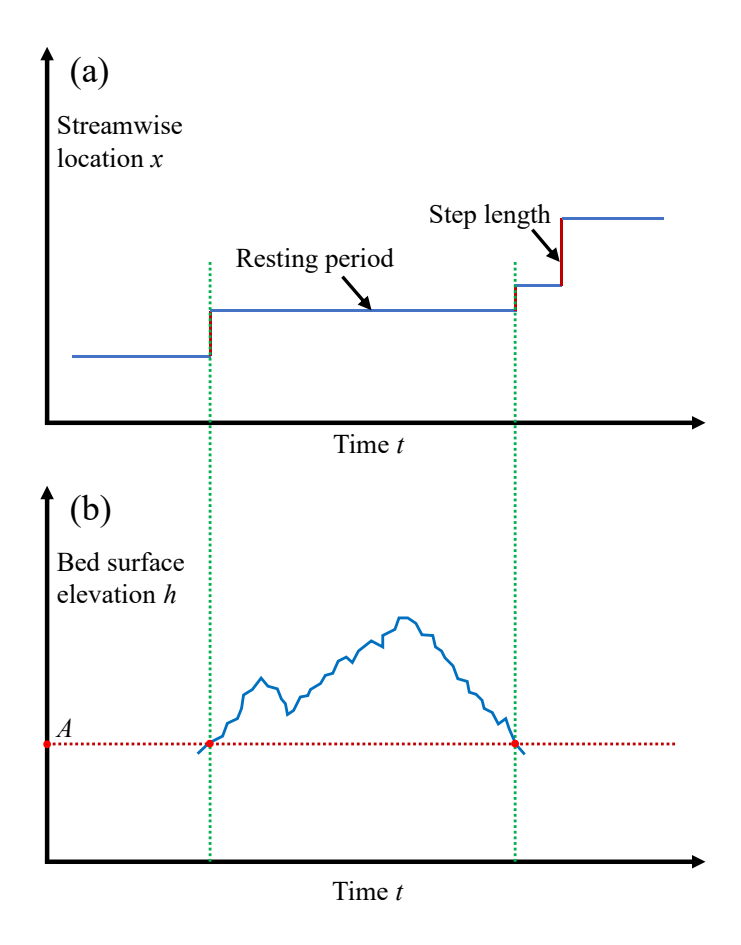


Figure 4: Sketch for resting times embedded in bed surface elevation series. (a) Alternating hops and resting periods for the transport of a bedload sediment particle tracer. Note that the steps are simplified for demonstration as instantaneous given normally their short durations compared to the long resting periods. (b) The corresponding bed surface elevation series for a specific resting period of the tracer.

Here we present the following algorithm to extract resting times.

- 1) For a bed elevation series $h(t_i)$ with $1 \le i \le N$, where N is the length of the series, we consider each of the record in the series from $h(t_1)$ to $h(t_N)$.
- 2) Note that we first detect the deposition event, followed by identifying the corresponding entrainment event for the same particle in the subsequent elevation series. This sequencing is crucial because if an entrainment event is detected first, indicating that a specific particle on the bed surface has been entrained and traveled downstream, there will be no subsequent deposition event recorded for this particle at that location. Thus, for each

elevation record $h(t_i)$ identified as the starting point in step 1), if $h(t_i) > h(t_{i+1})$, signifying an entrainment event, it implies that there is no corresponding deposition event for this particle in the remaining elevation series. Consequently, we proceed to consider the next record $h(t_{i+1})$, as outlined in step 1). Conversely, if $h(t_i) \le h(t_{i+1})$, we traverse the elevation series (from $h(t_{i+1})$ to $h(t_N)$) to identify the first record $h(t_{i+r})$ satisfying $h(t_i) > h(t_{i+r})$, indicating the occurrence of an entrainment event at $h(t_{i+r})$ for the particle previously deposited at $h(t_i)$. Hence, $(t_{i+r} - t_i)$ represents an instance of resting time.

3) Repeat the above procedure until the end of the bed elevation series.

With these extracted resting times, we obtain the exceedance probability distribution to analyze the tail characteristics.

3. Application of the FLM model for bed elevation fluctuations

3.1. Effects of the shape parameter v and the Hurst exponent H

Regarding application of the FLM model for the bed surface fluctuations, in this section we present details on how relevant parameters are estimated, and how these parameters can affect the model predictions, results of which demonstrate the potential of the model in correctly capturing the experimental observations.

The work by Ganti et al. (2009) applying the FLM model in the study of sediment transport series has proposed a straightforward means to estimate parameters of the model. Essentially, they attempted to preserve the multiscale characteristics in the measured time series, which is revealed by the structure functions, defined as

376
$$M(q,a) = \frac{1}{N-a} \sum_{t=1}^{N-a} |S(t+a) - S(t)|^q,$$
(7)

where q is the order of the structure function, S(t) is the sediment transport series, N is the length of series and a is the timescale. Since the constraints of matching the simulated and measured results of Eq. (7) are generally overdetermined (i.e. these constraints cannot be all satisfied), Ganti et al. (2009) chose to minimize the mean squared error between the simulated and measured scaling exponents for the first three orders of Eq. (7), giving estimates for the Hurst exponent H and the shape parameter v. By plotting those structure functions in the log-log plot and identifying the linear regions (for the scaling exponents) in the plot, the extracted scaling exponents are known to characterize the multifractality of the time series. Further matching the variances for the simulated and measured series gives the standard deviation σ for the model.

However, parameters estimated by the above method can be seen as having provided a "globally optimal" prediction for the FLM model across different timescales (regarding the measured series), instead of focusing on (or putting on more weight for) the model performance at some specific timescale. For our study concerning the effects of riverbed elevation variations on the streamwise bedload tracer particle transport, the most important process is the elevation variations at the finest timescale describing the detailed events on particles' deposition (elevation increases) and entrainment (elevation decreases), which can then be linked to the resting time distribution of particles (see the previous section 2.3). Thus, the priority in estimating the model parameters in the present study is to guarantee reproducing as close as possible the elevation increments at the finest timescale of a = 1, the PDF of which was demonstrated well approximated by the Laplace distribution Eq. (1) as shown in Figure 3 (a).

Although in Figure 3 we have compared results corresponding to both discharges of Q = 2000 and 2800 L/s to illustrate the intrinsic characteristics of multifractality (transition of PDF shape from Laplace to Gaussian as timescale increases), for brevity, the analysis hereinafter is only

401

402

403

404

405

406

407

408

409

410

411

412

413

414

415

416

417

418

419

420

421

422

based on that corresponding to Q = 2000 L/s due to qualitatively similar results exhibited for Q =2800 L/s. To estimate the parameters, we first analyze the effect of the shape parameter v in controlling the shape of the increments PDF. We note that the shape parameter v comes from the Gamma distribution of the increments of Gamma process, i.e. Eq. (4), which serves as the operational time for our considered subordinated stochastic process. Since the shape of Gamma distribution (with the scale parameter of unity) can be divided into three categories based on this shape parameter, i.e. v < 1, v = 1, and v > 1, we expect that the simulated PDF for the increments of bed elevations based on Eq. (2) will also be controlled by the same critical value of unity for v. For example, for the special case of v = 1, the Gamma distribution is simplified into an exponential distribution, based on which we could expect that the increments PDF of the FLM (with H = 0.5) can be described by the two-sided exponential distribution (or the Laplace distribution, Eq. (1)). Here we show in Figure 5 the PDFs of the bed elevation increments for the shape parameter v >1 (Figure 5 a and b) and v < 1 (Figure 5 c and d). It is obvious that the variation of the shape of the PDFs follows the same pattern as that of the Gamma distribution. That is, around the area of $\Delta h = 0$ the distribution becomes "flatter" for v > 1, while "spikier" for v < 1. These shapes may be characterized by the indicator of kurtosis, commonly defined as the 4th order moment. In general, Figure 5 provides information for estimating FLM parameters. Specifically, for a Hurst exponent of (or close to) 0.5, the shape parameter ν should be equal to (or close to) unity for the Laplace distribution of increments PDF at the finest timescale. In addition, the Hurst exponent (or correlation parameter) is well known for characterizing how the increments of the fBM are correlated across scales. If the magnitude of fluctuations are independent, the fBM reduces to the classic Brownian motion with H = 0.5. As discussed earlier, Hurst exponent in the

range of (0, 0.5) indicates a negative correlation while a positive correlation in the range of (0.5, 1). Mathematically, 2H can be related to the scaling exponent of the second order moment of the increments (Singh et al., 2011), which is a special case (q = 2) of Eq. (7):

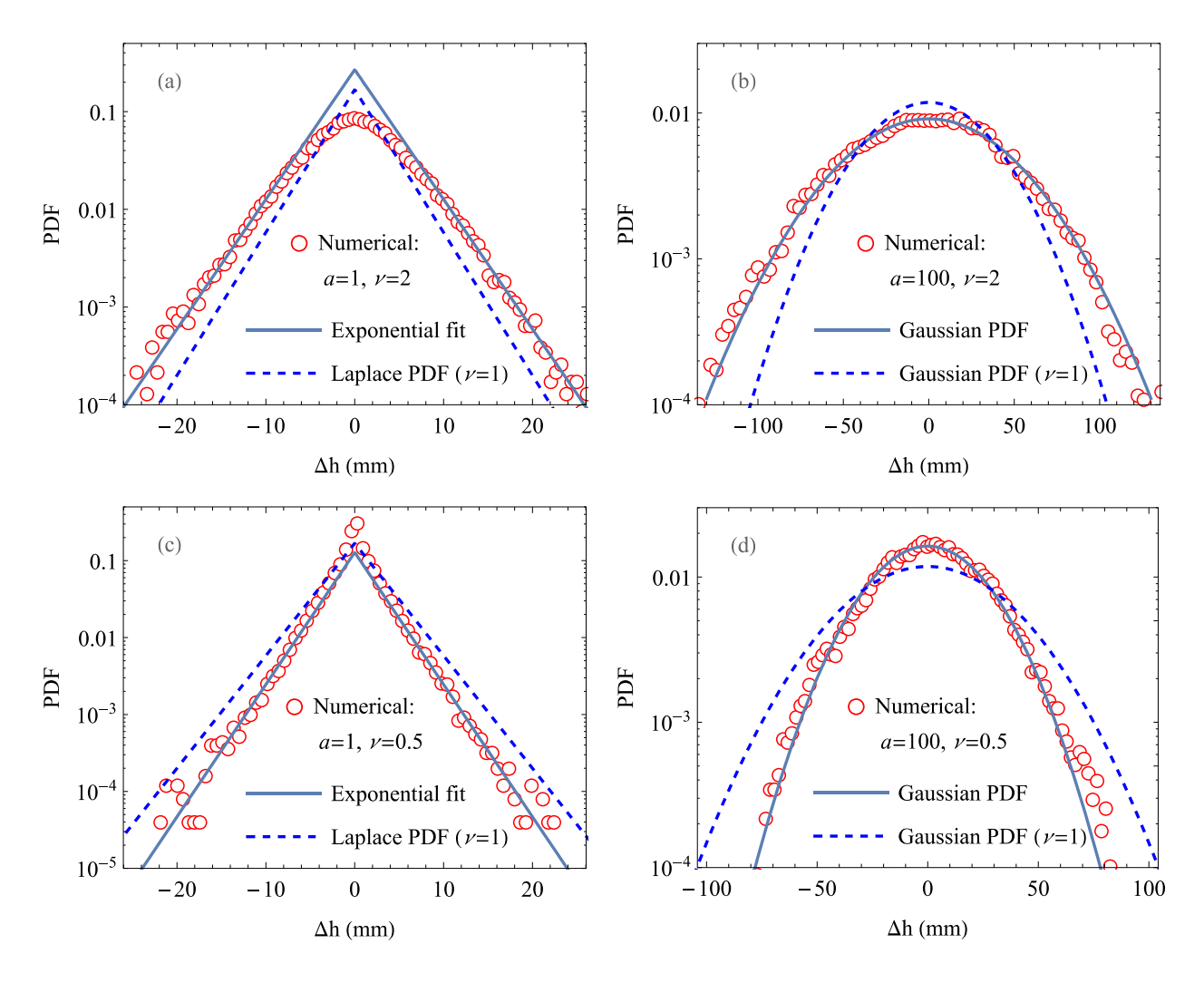


Figure 5: Effects of v on PDFs of bed elevation increments simulated by the FLM model. The other parameters are H = 0.5 and $\sigma = 4.2$ mm. Note that the solid blue lines in (a) and (c) represent exponential fits to numerical results instead of PDFs.

430
$$M(2,a) = \frac{1}{N-a} \sum_{t=1}^{N-a} |h(t+a) - h(t)|^2,$$
 (8)

where h(t) is the bed elevation series. In Figure 6 we fitted a straight line to the second order moment of the measured elevation series at the discharge of 2000 L/s with the slope of 0.9,

resulting in an estimation for the Hurst exponent H=0.45, charactering the manner based on which the variance of the increments should increase across different timescales. Note that in the earlier study of Singh et al. (2011) based on the analysis of power spectral density for the bed topography, the spectral slope $\beta=1.92$ was reported for the 2000 L/s case, which corresponds to an estimate of $H=(\beta-1)/2=0.46$, consistent with the present result of H=0.45.

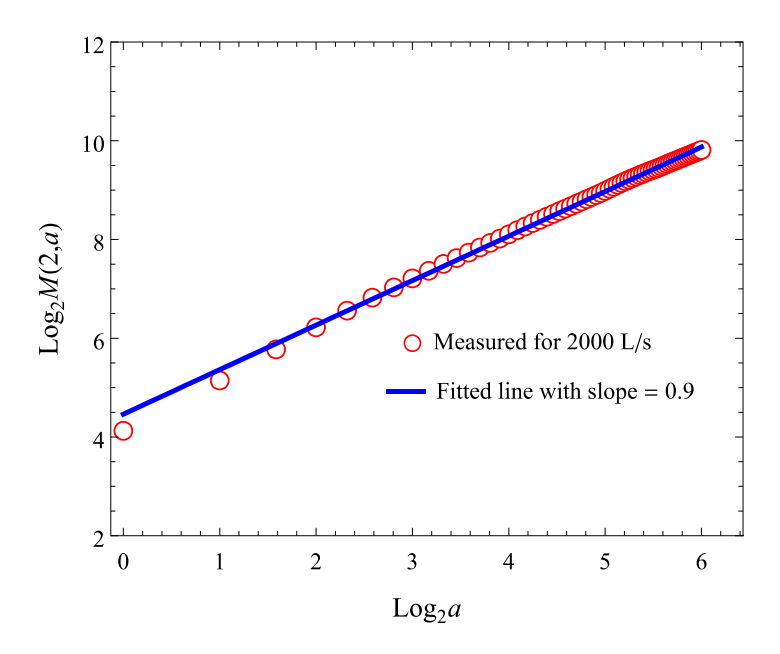


Figure 6: Estimating the Hurst exponent H based on the second order moment as defined by Eq. (8). The scaling exponent (slope of the fitted line in the log-log plot) is equal to 2 H.

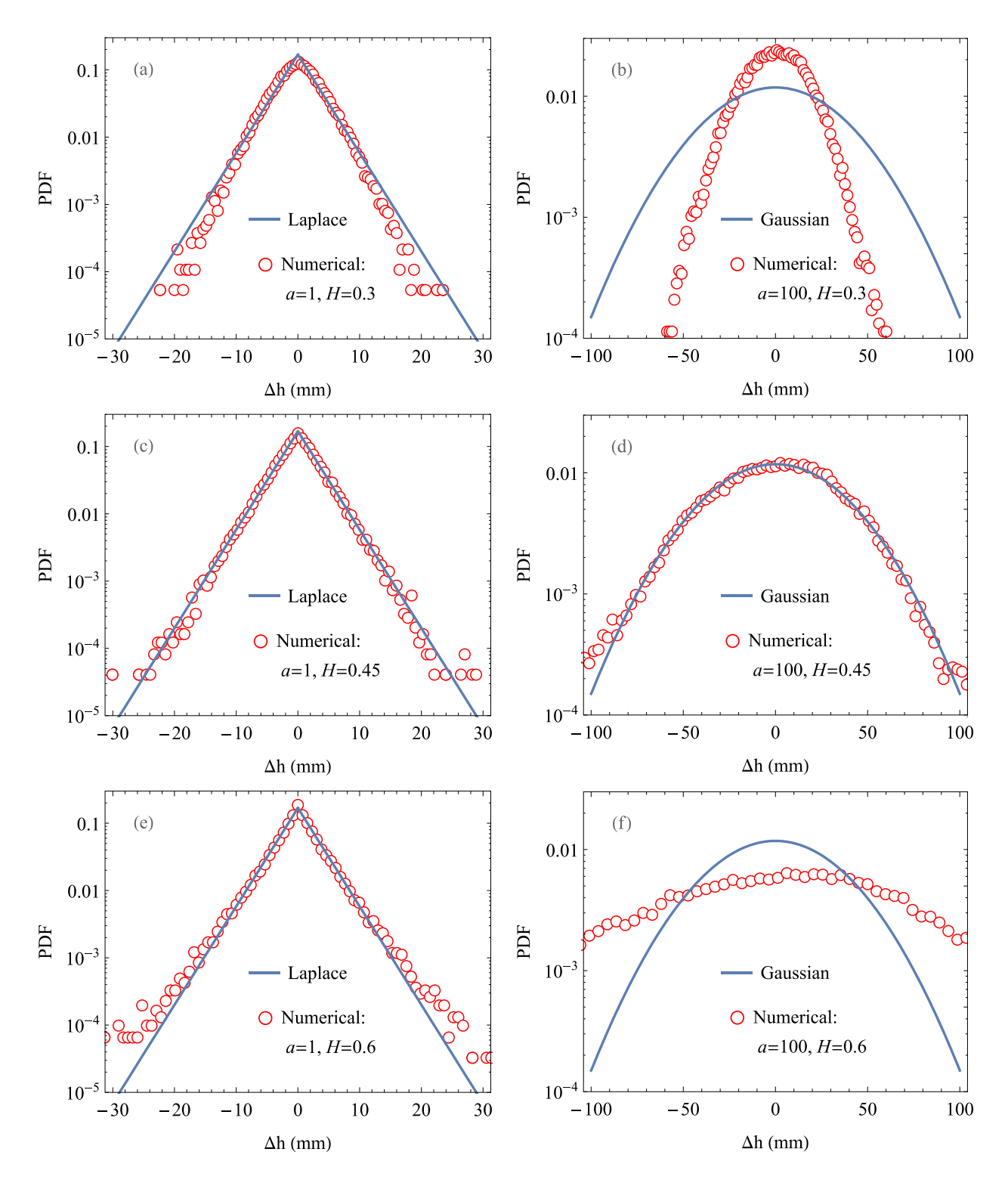


Figure 7: Effects of the Hurst exponent H on the PDF of elevation increments at two different timescales of a = 1 and a = 100, respectively. For the numerical simulations $\sigma = 4.2$ mm and v = 1 are used.

445

446

447

448

449

450

451

452

453

454

455

456

457

458

459

460

461

462

463

464

465

466

Given that H = 0.45 is close to H = 0.5, we can use the guess of v = 1 (as discussed above) for further analysis. The last parameter σ can be determined by computing the standard deviation of the elevation increments at the finest timescale of a = 1 referring to our proposed constraint of capturing as much information as possible regarding the increments PDF at this timescale. The value of $\sigma = 4.2$ mm is obtained from the experimentally measured bed elevation series at the discharge of 2000 L/s. In Figure 7, we show the results of numerical simulations based on the FLM model Eq. (2) to further illustrate the effects of the Hurst exponent H. The first observation is that as H increases from 0.3 to 0.6, the value of H does not affect much the variance of increments PDF at the finest timescale of a = 1 (Figure 7 a, c, and e), but significantly for that at the larger timescale of a = 1100 (Figure 7 b, d, and f). In addition, the dependence of the variance on H is monotonic, i.e. the variance increases as H increases, regardless of the timescale at which we are analyzing. Also observed is that the variance at the larger timescale of a = 100, resulted from a specific value of H (= 0.45) in the numerical simulation, agrees with that by the experimental measurements (represented by the blue Gaussian solid line). In fact, the understanding of 2H being the scaling exponent (or slope in the log-log plot) of Eq. (8) explains most of the observations regarding Figure 7. For example, since the variance (related to the second order moment) of the increments increases in a power-law manner across timescales, it consequently has a greater value at a larger timescale, the value of which depends monotonically on the Hurst exponent H. In field studies of gravel-bed rivers, it has been observed that the distribution of scour and fill depths during floods follows an exponential distribution (Haschenburger, 1999, 2006; Hassan & Church, 1994; Vázquez-Tarrío et al., 2021). These measurements of scour and fill depths bear similarities to the bed elevation increments examined in this paper but on a different timescale.

Moreover, the observed exponential distributions for scour and fill depths align with the Laplace distribution discussed in this study. This suggests the potential applicability of the FLM model to analyze scour and fill depths observations. However, a more detailed analysis of field data is necessary, including an examination of whether these observations exhibit multifractal behavior. Additionally, further validation of these results may require observations of tracer transport processes.

3.2. Gaussian PDF of elevation increments at the finest timescale (a = 1)

In this section, we show that the FLM model can also reproduce results with monofractal characteristics, further validating its ability to capture experimental observations.

It is known that FLM exhibits multifractal behavior (i.e. the increments PDF changes its shape across scales) only at some intermediate timescales, while revealing a monofractal behavior at the limit of very large timescales with the Gaussian increments PDF (Ganti et al., 2009; Kozubowski et al., 2006). However, results of Figure 5 (a) and Figure 7 (e) suggest that FLM may also approach a monofractal model under conditions of very small H or very large v. We provide two examples in Figure 8 adopting a small Hurst exponent H = 0.1 (Figure 8a) and a large shape parameter v = 10 (Figure 8b), respectively, where both the elevation increments PDFs are very close to Gaussian at the finest timescale of a = 1. To quantitatively evaluate the normality of results in Figure 8, we provide Quantile-Quantile plots in Figure 9 demonstrating how well these PDFs can be approximated by Gaussian distributions (Figure 9 a and c), as compared with cases for a larger H (= 0.3, Figure 9b; see Figure 7a for the PDF) or a smaller v (= 2, Figure 9d; see Figure 5a for the PDF), respectively.

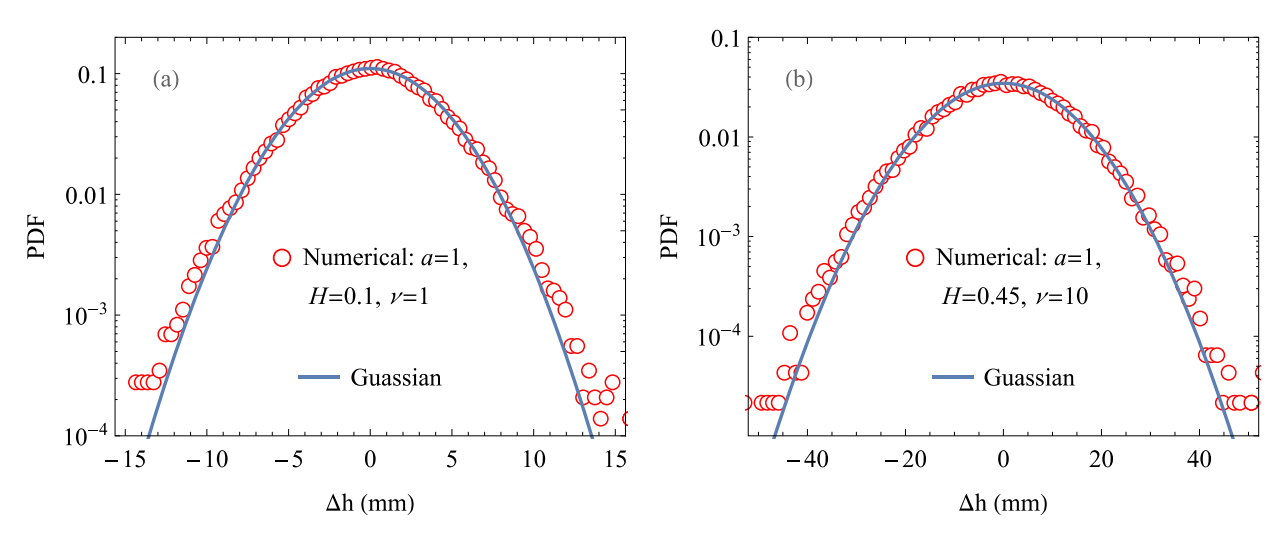


Figure 8: The Gaussian PDF for the elevation increments at the finest timescale of a = 1, which is achieved by adopting either a small Hurst exponent H = 0.1 (relative to 0.5), or a large shape parameter v = 10 (relative to 1). $\sigma = 4.2$ mm is used in the numerical simulations.

This characteristics of monofractality for the FLM model is important in the sense that it demonstrates the capability of the model in reproducing some previous results where multifractality is not observed, either experimentally (Martin et al., 2014) or numerically (Pierce & Hassan, 2020b). Bed elevation series captured in those studies show strong negative correlations implying possibly small values of H (close to zero), leading to resting time distributions with scaling exponents close to -1 for their power-law tails, which is consistent with corresponding results (Martin et al., 2014; Pierce & Hassan, 2020b).

Here we explain the observed monofractal behavior regarding the shape parameter v by resorting to the analytical solutions of the structure functions for FLM (Ganti et al., 2009; Kozubowski et al., 2006):

502
$$M(q,a) = \sqrt{\frac{2^q}{\pi}} \Gamma\left(\frac{1+q}{2}\right) \frac{\Gamma(H \ q+a \ v)}{\Gamma(a \ v)}. \tag{9}$$

It is known that at the limit of very large timescales (i.e. a is large) FLM is monofractal (Ganti et al., 2009; Kozubowski et al., 2006), effectively resulting in a large value for the product of $a \cdot v$ in

Eq. (9), which is equivalent to a large value of v as we found by Figure 9 c and d. However, we note that this could not explain the effect of a small H in inducing the observed monofractality, which needs further investigation.

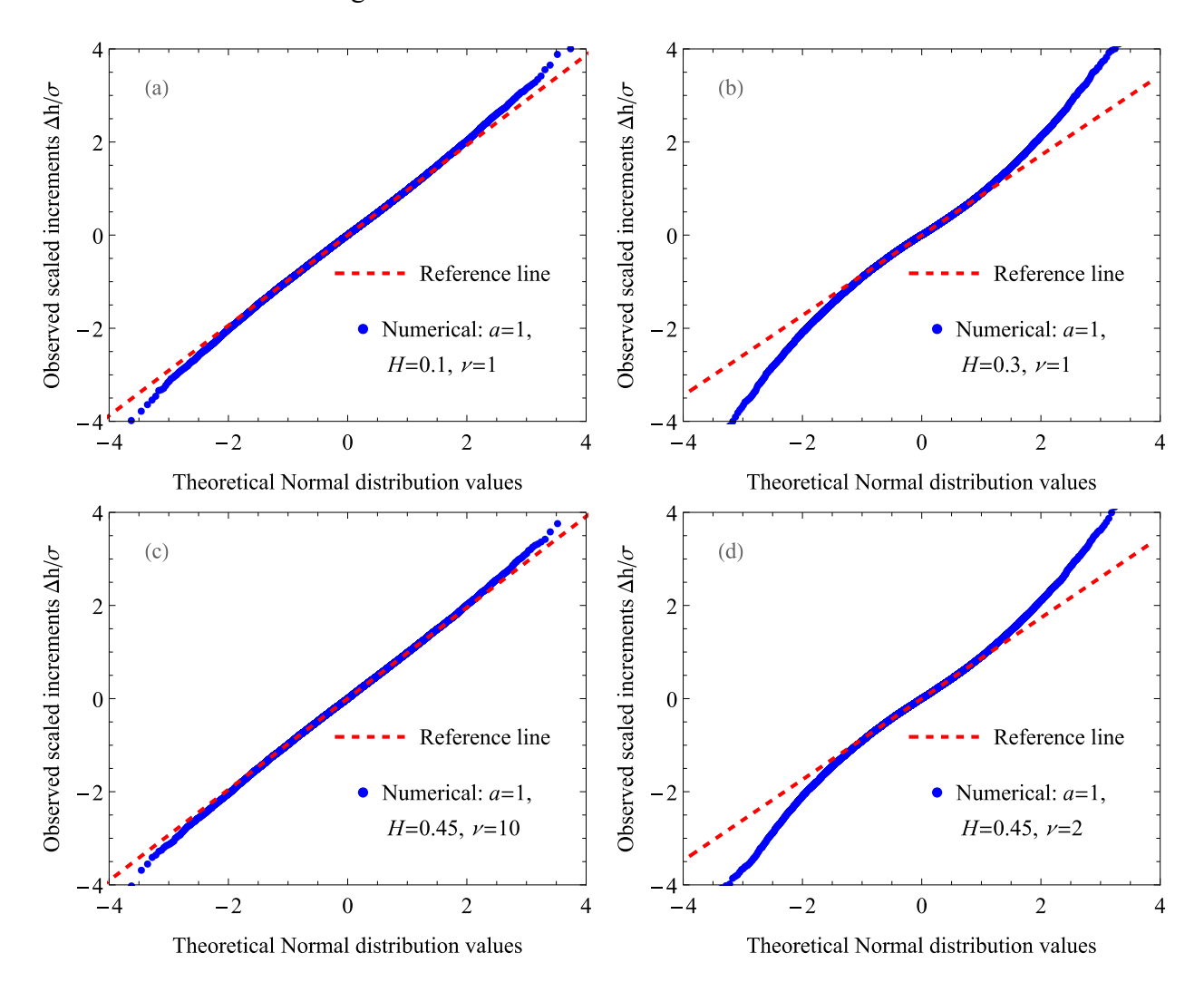


Figure 9: Quantile-Quantile plot illustrating that as the decrease of the Hurst exponent H from 0.3 to 0.1, or increase the shape parameter v from 2 to 10, the PDF of the elevation increments approaches Gaussian. The dashed red line (Reference line) indicates Gaussian distribution.

3.3. Effects of the dataset size N

In practice, it is always interesting to understand if an empirical series contains sufficient size of data to support meaningful analysis. That is, whether robust results can be obtained based on the limited-length empirical series. However, different means of the analysis may lead to

different answers, as we are going to demonstrate here and in the next subsection in estimating

516

the FLM model parameters, based on the variance of the increments PDF and the scaling 517 exponent of the tail of the resting time distribution, respectively. 518 With our estimated parameters in the previous subsections (H = 0.45, v = 1, and $\sigma = 4.2$ mm), 519 we compare the FLM model results of bed elevation increments PDF with the experimental 520 measurements at two different timescales in Figure 10, illustrating the effects of dataset size N on 521 the distributions. The first set of model results (Figure 10 a and b) are based on the dataset size of 522 $N = 4 \times 10^4$, which is consistent with that used for previous figures of model simulations in this 523 paper. In addition, a different dataset size of $N = 4 \times 10^3$, which is an order of magnitude smaller 524 and represents the size of the experimentally measured series, is adopted for Figure 10 c and d. 525 Overall, Figure 10 gives us confidence that the model results reproduce closely the 526 experimental measurements regarding the increments PDF. The dataset size of $N = 4 \times 10^3$ may 527 not be sufficient to guarantee a stable distribution of the PDF at the timescale of a = 100, but it 528 generates results with stable statistical information like the variance. In other words, the 529 simulated increments PDF changes for each realization (more profoundly at the larger timescale; 530 and the experimental results can be seen as one special realization) with this smaller dataset size, 531 however the changes for the variance of the PDF are very small, which supports a robust 532 estimation of the parameters as we obtained in this study for the Hurst exponent H. With the 533 increase of the dataset size to $N = 4 \times 10^4$, the shape of the PDF is stabilized (Figure 10b), i.e., no 534 535 significant changes in PDF shape among different realizations. We emphasize that through the preceding steps, the FLM model is appropriately calibrated to 536 capture the observed elevation characteristics (Figure 10c and d). While the experimental data 537 inevitably faces the "censorship problem" (Ballio et al., 2019), we can address this limitation by 538

increasing the sample size in the numerical simulation (Figure 10a and b). This step is crucial for the subsequent analysis of resting time distribution, as the distribution's exact nature is unknown due to insufficient experimental observations.

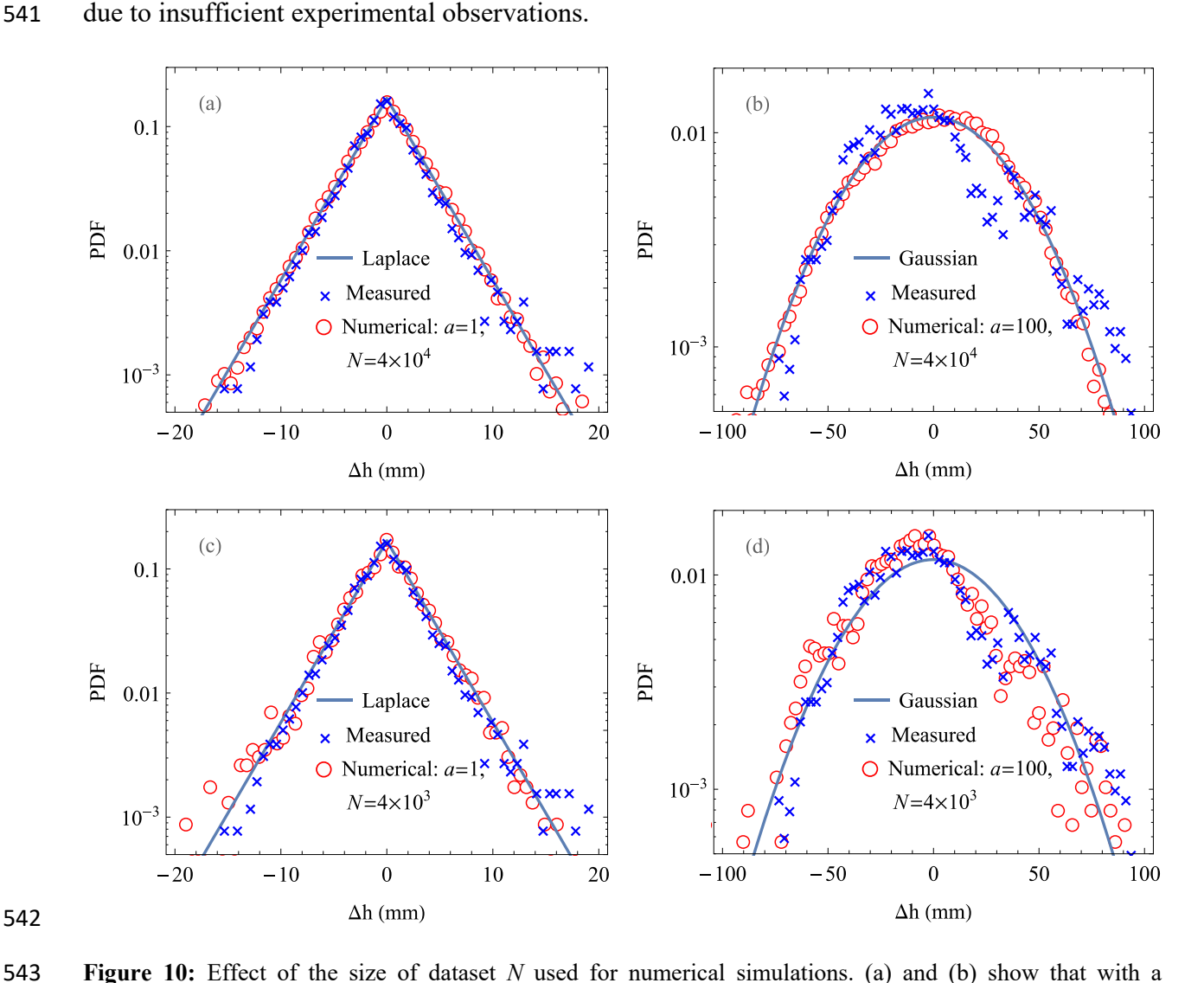


Figure 10: Effect of the size of dataset N used for numerical simulations. (a) and (b) show that with a relatively large N the simulated results can be accurately fitted by the Laplace distribution and Gaussian distribution at the finest timescale of a = 1 and a larger timescale of a = 100, respectively. With (c) and (d) we demonstrate that using a smaller N which is the same as that for the experimentally measured elevation variation time series, the simulated results at the larger timescale can change profoundly. Note that we selected a realization of the numerical simulation which agreed closely in shape with the experimental results (d). Also we note that variances do not change much for corresponding simulations with different N, demonstrating that variance can be used to robustly estimate the model parameters.

4. Tails of the resting time distribution

551

552

553

554

555

556

557

558

559

560

561

562

563

564

565

566

567

568

569

570

571

572

573

Using the algorithm described in subsection 2.2, we can extract resting times embedded in the elevation series. We first show results of the exceedance probability distribution for the experimental data at the discharge of 2000 L/s in Figure 11 a, where a reference line fitted to the part of the tail close to the end of the distribution is shown with a scaling exponent of -0.705. This distribution is truncated around the time at the order of $\sim 10^3 \times 5$ s, where 10^3 is related to the size of the collected dataset and 5s is the sampling interval of measurements. It has been suggested that the exceedance distribution of resting times as described by the term of "return time" for the fractional Brownian motion decays as $\sim t^{H-1}$ (Ding & Yang, 1995; Voepel et al., 2013), relating the scaling exponent of the tail of the resting time distribution to the Hurst exponent. Thus, the measured results in Figure 11a should indicate a value of Hurst exponent of H = 0.3, which is very different from the value of H = 0.45 estimated from the experimental observations (see Figure 6 and discussions thereafter). However, by the other three subfigures (b, c, d) in Figure 11 we demonstrate that this observed discrepancy between two estimated Hurst exponents based on different means are simply due to insufficient data in the collected series. Using $N = 4 \times 10^3$ representing dataset size of the measured data, we repeat the numerical simulations based on the FLM model and pick out three realizations showing different scaling exponents for the exceedance probability distributions. The result can either be very close to the experimental measurements (Figure 11b), or show a heavier (Figure 11c) or a thinner (Figure 11d) tail than that in Figure 11a. Nevertheless, in the case of insufficient data for analysis, the slope of the tail is seen directly dependent on the order of magnitude of time when the resting time distribution is truncated (due to randomness in numerically generating the bed elevation series). For example, the larger timescale for the

truncation of the distribution, the heavier the tail of the distribution is (Figure 11 d, b, and c). Furthermore, for the special case of the same truncation timescale regarding both resting time distributions obtained experimentally and numerically (Figure 11 b), we observe great agreement between the two distributions (thus the same tail slope), implying the ability of the FLM model in reproducing correct resting times related to capturing characteristics of bed elevation series. This observation indicates that different tail behaviors of the bed elevation increments PDF (power-law as documented in Singh et al. (2012b) vs. exponential as described in this paper) may not significantly affect the resting time distribution.

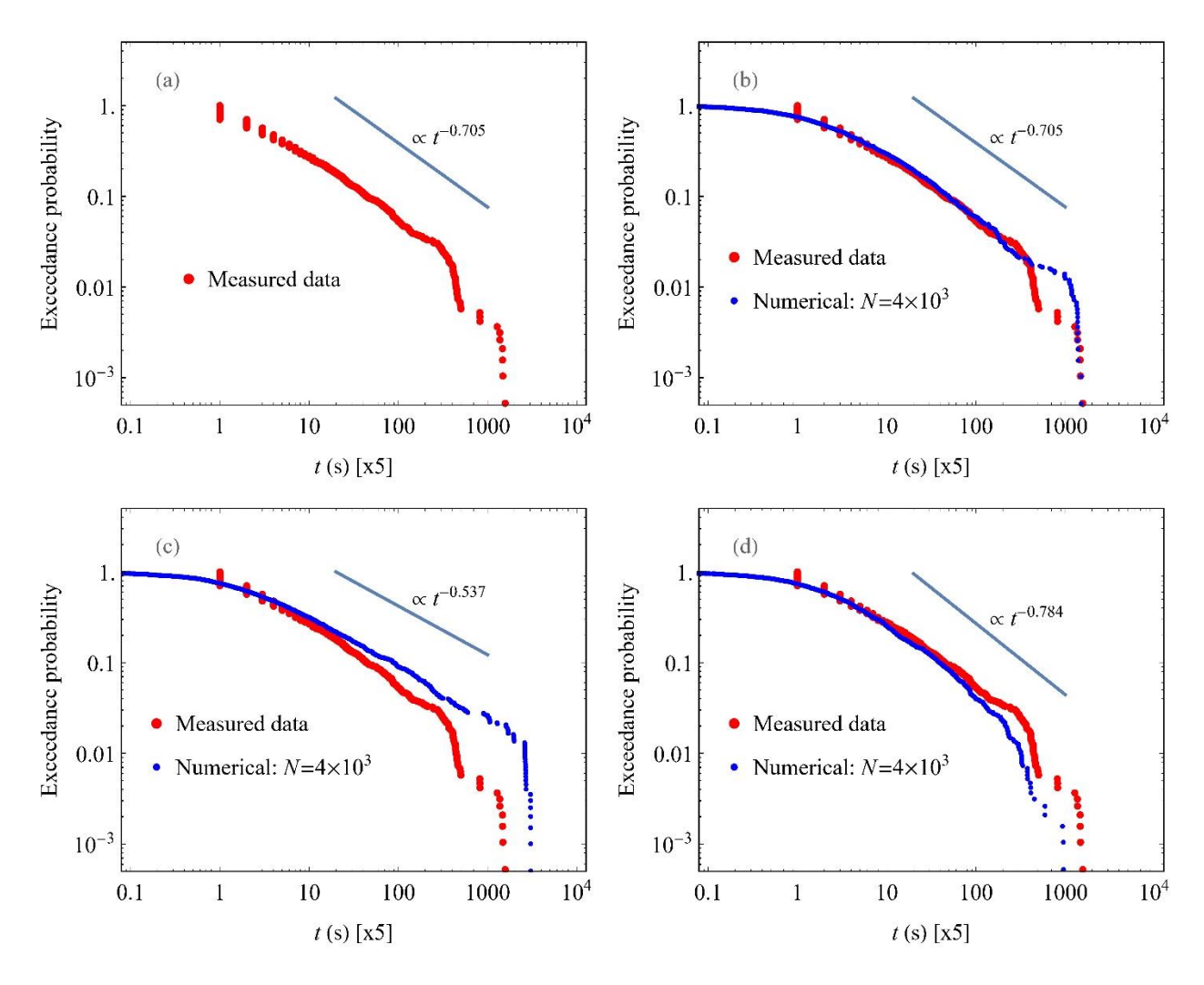


Figure 11: Exceedance probability distribution for resting times of particles extracted from bed elevation series with N = 4000. (a) The experimentally measured elevation series under the discharge of 2000 L/s. (b) A

selected realization of the numerical simulation which closely agree with the experimental measurements. (c) and (d) show realizations of numerical simulations with tails of the resting time distributions vary, which can either be milder (c), or steeper (d) than the measurements.

We continue to increase the size of the dataset used for the simulation to $N = 1 \times 10^5$, slightly over an order of magnitude larger than that for the experiment and obtain the exceedance probability distribution. The resulting slope of the distribution in the log-log plot are found much more consistent, the scaling exponents of which are around -0.55, as that plotted in Figure 12. This result emphasizes that cautions should be used in estimating the Hurst exponent by the resting time distribution, a robust estimation of which may require a large dataset and could be beyond the size of the empirically collected dataset.

We need to emphasize that the Hurst exponent H=0.45 in this study represents an "effective Hurst exponent" because we relate the scaling of the second order moment Eq. (8) to 2H, i.e. M (2, a) $\sim a^{2H}$, the form of which is monoscaling (corresponds to monofractality for the elevation series). A general form of M (q, a) $\sim a^{\tau(q)}$ can be adopted for the multiscaling case, with a quadratic relation normally used for the spectrum of scaling exponents $\tau(q) = c_1 q - c_2 q^2 / 2$, where q is the order of the moment, and c_1 and c_2 are two scaling exponents; c_2 is commonly referred to as the intermittency coefficient and characterizes multifractality (i.e. measure the departure from mono-scaling (Singh et al., 2011)) in a series. Thus, it is easy to find that rather than simply c_1 (for the mono-scaling), the Hurst exponent is further modified by c_2 , as $H=c_1-c_2$. More specifically, we can obtain $c_1=0.56$ and $c_2=0.11$ for the experimental results collected under the discharge of 2000 L/s for timescales between a=1 and $a=2^6$, compared with values of 0.53 and 0.12 in Singh et al. (2011), respectively.

We highlight that the scaling exponent of -0.55 (= H - 1) for the resting time distribution identified here from the FLM model based on the experiment observations (2000 L/s) indicates a

much heavier tail than that estimated in previous studies (scaling exponent of around -1.0 (Martin et al., 2014; Pierce & Hassan, 2020b)), suggesting that the noted difference is due to multifractal behavior observed in the bed surface elevation series.

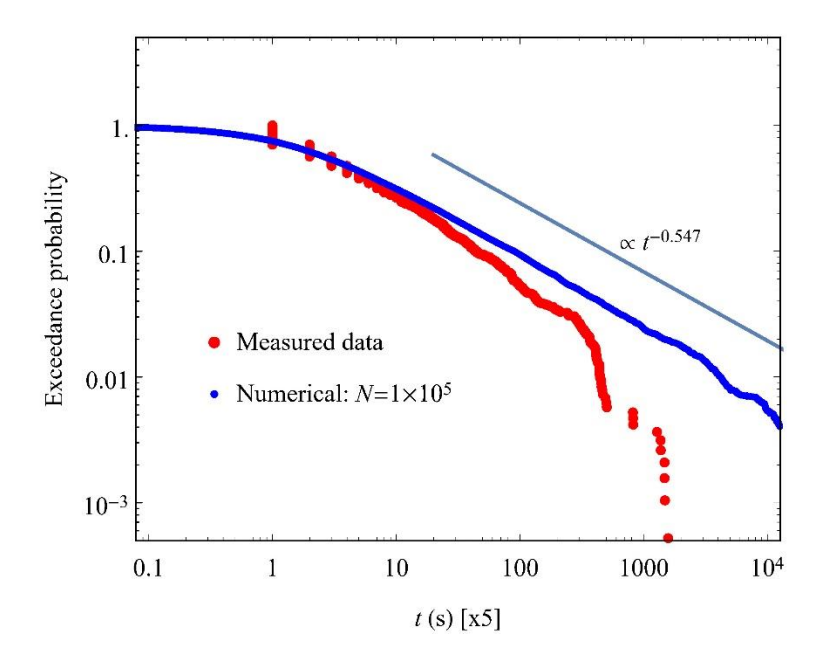


Figure 12: Exceedance probability distribution for resting times of particles extracted from bed elevation series. Adopting an order of magnitude larger $N = 1 \times 10^5$ than that in Figure 11, results by the numerical simulations converge to the resting time distribution with the scaling exponent of \sim -0.55 for the tail, which is much heavier than that obtained in previous studies (Martin et al., 2014; Pierce & Hassan, 2020b) without observing the multifractality in the bed elevation series.

5. Summary and conclusion

The Fractional Laplace Motion (FLM) model is known to exhibit multifractal behavior in the generated spatial or temporal series, which capture a gradual change of the shape of increments PDF from the Laplace to the Gaussian distribution as the considered scale increases. In the field of sediment transport, this model has been applied to study the sediment transport series in observation of similar multifractal behaviors. In this paper, we explore the FLM model in simulating bed elevation fluctuations, which is closely related to the process of bedload tracer particle transport by providing a means of obtaining the resting times of particles when they

temporarily stop their motions in the course of downstream transport. However, we primarily considered reproducing the elevation increments PDF at the finest timescale as the constraints in estimating model parameters, which is different from the previous study for sediment transport series which focused on minimizing the difference between the simulated and measured time series regarding some multiscale characteristics across timescales.

To assist parameters estimation, we have investigated effects of different parameters. The shape parameter v emerges from the operational time of Gamma process (with the scale parameter of unity) for the subordinated stochastic process and affects the shape of the increments PDF in a similar way of affecting the Gamma distribution. Qualitatively, compared with the exponential distribution, the PDF becomes "spikier" close to the mode of the distribution for v < 1, and "flatter" for v > 1, when the Hurst exponent H is close to 0.5. Mathematically, H can be related to the scaling exponent of the second order moment of the increments; it affects the shape of the PDF in a similar manner as v. We demonstrate that under conditions of smaller H (than 0.5) or larger v (than 1), the shape of the increments PDF at the finest timescale approaches Gaussian (i.e. monofractality), indicating that the FLM model is capable of reproducing previous experimental and numerical results with respect to which multifractal behaviors are not observed.

Bed elevation increments at the finest timescale describe detailed events of particle entrainment and deposition, which are key in resolving resting times of particles. In this paper, we use essentially the same empirical method by Voepel et al. (2013) to extract resting times from a given elevation time series, which is based on identifying pairs of adjacent deposition and entrainment events at the same elevation. Results show that the FLM model can reproduce resting times observed in experiments: the exceedance probability distributions for the simulated

and measured elevation series agree satisfactorily with each other. However, our model simulations also demonstrated that in case of insufficient size of the dataset, the slope of the tails of resting time distribution in the log-log plot can vary profoundly, leading to uncertainties in estimating Hurst exponent focusing on the tail characteristics under such circumstances. Therefore, we emphasize that caution should be made in estimating the model parameters concerning the size of the dataset. For example, although the shape of the increments PDF may not be stable for insufficient data at some large timescale, the variance of the PDF can still be converged for different realizations of the numerical simulation based on the FLM model, which can guarantee a robust estimation of the parameter like the Hurst exponent, in contrast to that done through the tails of the resting time distribution. We note that due to the observed multifractality for bed surface elevation series in the considered experimental measurements, the calculated resting time distribution has a much heavier tail with the exponent of \sim -0.55, compared with previous results of \sim -1.0 for the elevation series showing monofractal behaviors. This work can be seen as a step towards relating the micro-scale particle dynamics to the macroscale sediment transport statistics via minimum complexity stochastic models.

Acknowledgement

649

650

651

652

653

654

655

656

657

658

659

660

661

662

663

664

665

666

667

668

669

This work is partially supported by the National Key Research and Development Program of China (2021YFC3200402), the National Natural Science Foundation of China (U2243222, U2243240, and 52179067), and the National Science Foundation (EAR-1854452). We acknowledge fruitful discussions with Mark Meerschaert and Niannian Fan at the initial stage of the preparation of this manuscript. We also thank the Editor A.J.F. (Ton) Hoitink, the Associate

- 670 Editor Luca Solari, and three anonymous reviewers whose suggestions and comments
- substantially improved our presentation and refined our interpretations.

Open Research

672

674

The data used in this study can be downloaded from the repository of Zenodo (Singh, 2024).

References

- Aberle, J., & Nikora, V. (2006). Statistical properties of armored gravel bed surfaces. Water Resources
- 676 Research, 42(11), W11414.
- Aberle, J., Nikora, V., Henning, M., Ettmer, B., & Hentschel, B. (2010). Statistical characterization of bed
- 678 roughness due to bed forms: A field study in the Elbe River at Aken, Germany. Water Resources
- 679 Research, 46(3), W03521.
- 680 Ballio, F., Radice, A., Fathel, S. L., & Furbish, D. J. (2019). Experimental Censorship of Bed Load Particle
- Motions, and Bias Correction of the Associated Frequency Distributions. Journal of Geophysical
- 682 *Research: Earth Surface*, 124, 116-136.
- Best, J. (2005). The fluid dynamics of river dunes: A review and some future research directions. Journal of
- *Geophysical Research: Earth Surface*, 110(F4), F04S02.
- Bradley, D. N. (2017). Direct Observation of Heavy-Tailed Storage Times of Bed Load Tracer Particles
- Causing Anomalous Superdiffusion. *Geophysical Research Letters*, 44(24), 227-235.
- 687 Coleman, S. E., & Melville, B. W. (1994). Bed-form development. *Journal of Hydraulic Engineering*, 120(5),
- 688 544-560.
- 689 Ding, M., & Yang, W. (1995). Distribution of the first return time in fractional Brownian motion and its
- application to the study of on-off intermittency. *Physical Review E*, 52(1), 207.
- 691 Einstein, H. (1937). Bedload transport as a probability problem. Sedimentation (reprinted in 1972). Water
- *Resources Publications, Colorado*, 105-108.
- Einstein, H. A. (1950), The bed-load function for sediment transportation in open channel flows, US
- Department of Agriculture Washington, DC.
- 695 Ganti, V., Lamb, M. P., & McElroy, B. (2014). Quantitative bounds on morphodynamics and implications for
- reading the sedimentary record. *Nature communications*, *5*, 3298.
- 697 Ganti, V., Singh, A., Passalacqua, P., & Foufoula-Georgiou, E. (2009). Subordinated Brownian motion model
- for sediment transport. *Physical Review E*, 80(1), 011111.
- 699 Guala, M., Singh, A., BadHeartBull, N., & Foufoula-Georgiou, E. (2014). Spectral description of migrating
- 700 bed forms and sediment transport. Journal of Geophysical Research: Earth Surface, 119(2), 123-137.

- 701 Haschenburger, J. K. (1999). A probability model of scour and fill depths in gravel bed channels. Water
- 702 Resources Research, 35(9), 2857-2869.
- Haschenburger, J. K. (2006). Observations of event based streambed deformation in a gravel bed channel.
- 704 Water Resources Research, 42(11).
- 705 Hassan, M. A., & Church, M. (1994). Vertical mixing of coarse particles in gravel bed rivers: A kinematic
- 706 model. *Water Resources Research*, *30*(4), 1173-1185.
- Hassan, M. A., Voepel, H., Schumer, R., Parker, G., & Fraccarollo, L. (2013). Displacement characteristics of
- 708 coarse fluvial bed sediment. *Journal of Geophysical Research: Earth Surface*, 118(1), 155-165.
- Jerolmack, D. J., & Mohrig, D. (2005). A unified model for subaqueous bed form dynamics. Water Resources
- 710 Research, 41(12), W12421.
- Jiang, W., Zeng, L., Fu, X., & Wu, Z. (2022). Analytical solutions for reactive shear dispersion with boundary
- adsorption and desorption. *Journal of Fluid Mechanics*, 947, A37.
- 713 Khosronejad, A., & Sotiropoulos, F. (2017). On the genesis and evolution of barchan dunes: morphodynamics.
- 714 *Journal of Fluid Mechanics*, *815*, 117-148.
- 715 Kozubowski, T. J., Meerschaert, M. M., & Podgorski, K. (2006). Fractional laplace motion. Advances in
- 716 *applied probability*, *38*(2), 451-464.
- 717 Lee, J., Singh, A., & Guala, M. (2022). Reconstructing sediment transport by migrating bedforms in the
- 718 physical and spectral domains. Water Resources Research, 58(7), e2022WR031934.
- 719 Li, G., Gong, Z., Jiang, W., Zhan, J., Wang, B., Fu, X., Xu, M., & Wu, Z. (2023). Environmental transport of
- 720 gyrotactic microorganisms in an open-channel flow. Water Resources Research, 59(4), e2022WR033229.
- 721 Liu, M., Pelosi, A., & Guala, M. (2019). A statistical description of particle motion and rest regimes in open-
- 722 channel flows under low bedload transport. Journal of Geophysical Research: Earth Surface, 124(11),
- 723 2666-2688.
- 724 Martin, R. L., Jerolmack, D. J., & Schumer, R. (2012). The physical basis for anomalous diffusion in bed load
- transport. Journal of Geophysical Research: Earth Surface, 117(F1), F01018.
- 726 Martin, R. L., Purohit, P. K., & Jerolmack, D. J. (2014). Sedimentary bed evolution as a mean-reverting
- 727 random walk: Implications for tracer statistics. *Geophysical Research Letters*, 41(17), 6152-6159.
- 728 McElroy, B., & Mohrig, D. (2009). Nature of deformation of sandy bed forms. Journal of Geophysical
- 729 *Research: Earth Surface*, 114(F3), F00A04.
- 730 Meerschaert, M. M., Kozubowski, T. J., Molz, F. J., & Lu, S. (2004). Fractional Laplace model for hydraulic
- 731 conductivity. *Geophysical Research Letters*, 31(8), L08501.

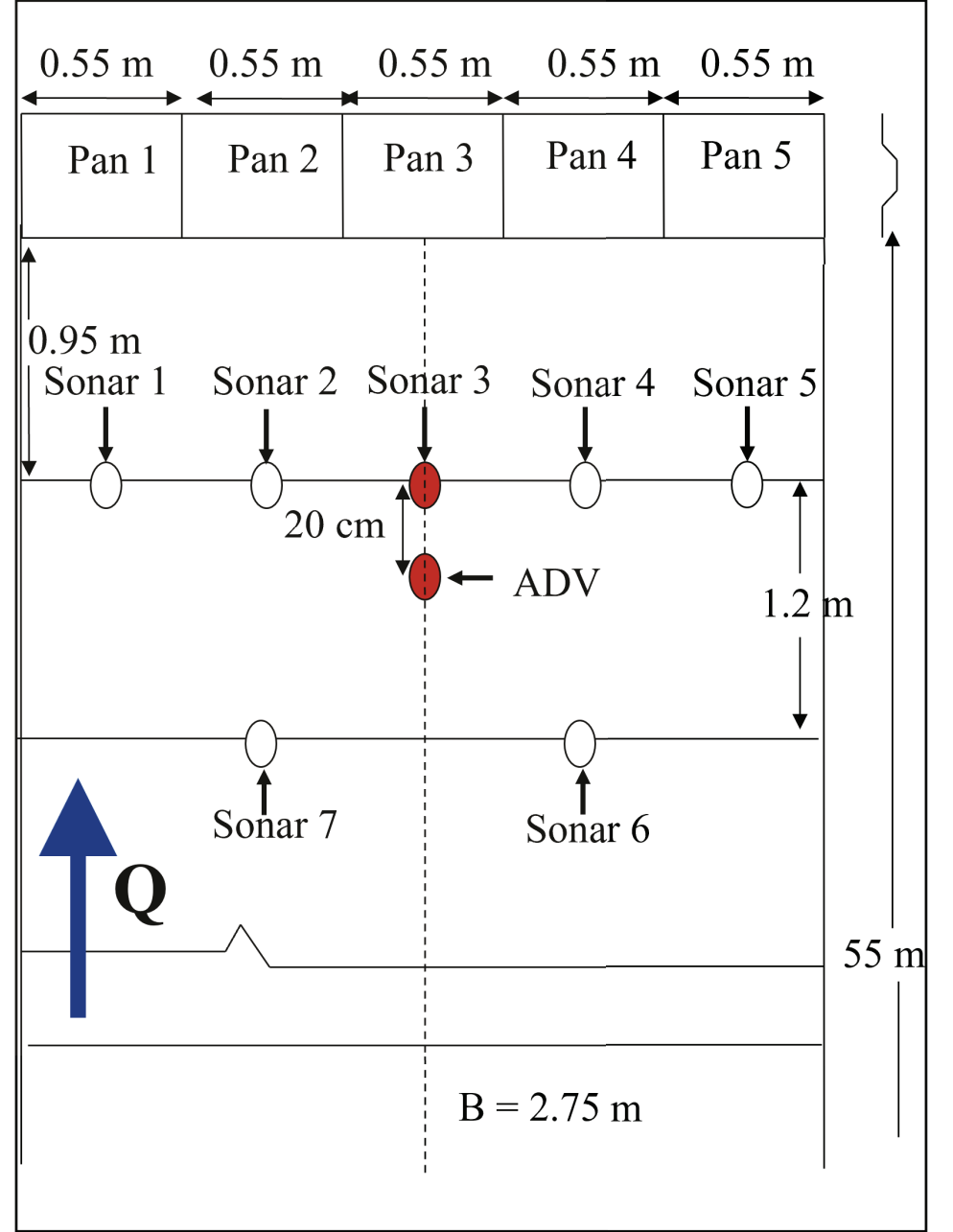
- Monsalve, A., Yager, E. M., & Schmeeckle, M. W. (2017). Effects of Bed Forms and Large Protruding Grains
- 733 on Near Bed Flow Hydraulics in Low Relative Submergence Conditions. Journal of Geophysical
- 734 Research: Earth Surface, 122(10), 1845-1866.
- 735 Nikora, V., & Walsh, J. (2004). Water-worked gravel surfaces: High-order structure functions at the particle
- scale. Water Resources Research, 40(12), W12601.
- 737 Nikora, V. I., Sukhodolov, A. N., & Rowinski, P. M. (1997). Statistical sand wave dynamics in one-directional
- water flows. *Journal of Fluid Mechanics*, *351*, 17-39.
- Parisi, G., & Frisch, U. (1985), On the singularity structure of fully developed turbulence, in *Turbulence and*
- 740 Predictability in Geophysical Fluid Dynamics and Climate Dynamics, edited by M. Ghil, North-Holland,
- 741 Amsterdam.
- Parker, G., & Wilcock, P. R. (1993). Sediment Feed and Recirculating Flumes: Fundamental Difference.
- 743 *Journal of Hydraulic Engineering*, 119(11), 1192-1204.
- Parsons, D. R., Best, J. L., Orfeo, O., Hardy, R. J., Kostaschuk, R., & Lane, S. N. (2005). Morphology and
- 745 flow fields of three-dimensional dunes, Rio Paraná, Argentina: Results from simultaneous multibeam
- echo sounding and acoustic Doppler current profiling. Journal of Geophysical Research: Earth Surface,
- 747 *110*(F4), F04S03.
- Pelosi, A., Schumer, R., Parker, G., & Ferguson, R. (2016). The Cause of Advective Slowdown of Tracer
- 749 Pebbles in Rivers: Implementation of Exner Based Master Equation for Coevolving Streamwise and
- 750 Vertical Dispersion. *Journal of Geophysical Research: Earth Surface*, 121, 623-637.
- 751 Pender, G., Hoey, T. B., Fuller, C., & Mcewan, I. K. (2001). Selective bedload transport during the
- degradation of a well sorted graded sediment bed. *Journal of Hydraulic Research*, 39(3), 269-277.
- 753 Pierce, J. K., & Hassan, M. A. (2020a). Back to Einstein: burial-induced three-range diffusion in fluvial
- sediment transport. *Geophysical Research Letters*, e2020GL087440.
- 755 Pierce, J. K., & Hassan, M. A. (2020b). Joint Stochastic Bedload Transport and Bed Elevation Model:
- 756 Variance Regulation and Power Law Rests. Journal of Geophysical Research: Earth Surface, 125(4),
- 757 e2019JF005259.
- 758 Ranjbar, S., & Singh, A. (2020). Entropy and Intermittency of River Bed Elevation Fluctuations. *Journal of*
- 759 *Geophysical Research: Earth Surface*, 125(8), e2019JF005499.
- 760 Schumer, R., Meerschaert, M. M., & Baeumer, B. (2009). Fractional advection-dispersion equations for
- modeling transport at the Earth surface. Journal of Geophysical Research: Earth Surface, 114(F4),
- 762 F00A07.

- Simons, D. B., & Richardson, E. V. (1962). Resistance to Flow in Alluvial Channels. *Transactions of the American Society of Civil Engineers*, 127(1), 927-954.
- Singh, A. (2024). Bed elevation (Version v2) [Dataset]. Zenodo, https://doi.org/10.5281/zenodo.10957926.
- Singh, A., Porté-Agel, F., & Foufoula-Georgiou, E. (2010). On the influence of gravel bed dynamics on
- velocity power spectra. Water Resources Research, 46(4).
- Singh, A., Lanzoni, S., Wilcock, P. R., & Foufoula-Georgiou, E. (2011). Multiscale statistical characterization
- of migrating bed forms in gravel and sand bed rivers. Water Resources Research, 47(12), W12526.
- Singh, A., Guala, M., Lanzoni, S., & Foufoula-Georgiou, E. (2012a). Bedform effect on the reorganization of
- surface and subsurface grain size distribution in gravel bedded channels. Acta Geophysica, 60, 1607-
- 772 1638.
- Singh, A., Foufoula-Georgiou, E., Porté-Agel, F., & Wilcock, P. R. (2012b). Coupled dynamics of the co-
- evolution of gravel bed topography, flow turbulence and sediment transport in an experimental channel.
- Journal of Geophysical Research: Earth Surface, 117(F4), F04016.
- 776 Singh, A., Wu, Z., Wilcock, P., & Foufoula-Georgiou, E. (2023). Experimental observations of bedload tracer
- movement: effects of mixed particle sizes and bedforms. Water Resources Research, 59(5),
- 778 e2022WR033114.
- Singh, A., Fienberg, K., Jerolmack, D. J., Marr, J., & Foufoula-Georgiou, E. (2009). Experimental evidence
- 780 for statistical scaling and intermittency in sediment transport rates. *Journal of Geophysical Research*:
- 781 *Earth Surface*, 114(F1), F01025.
- 782 Singh, A., Czuba, J. A., Foufoula-Georgiou, E., Marr, J. D., Hill, C., Johnson, S., Ellis, C., Mullin, J., Orr, C.
- 783 H., & Wilcock, P. R. (2013). StreamLab Collaboratory: Experiments, data sets, and research synthesis.
- 784 *Water Resources Research*, 49(3), 1746-1752.
- 785 Sotiropoulos, F., & Khosronejad, A. (2016). Sand waves in environmental flows: Insights gained by coupling
- large-eddy simulation with morphodynamics. *Physics of Fluids*, 28(2), 021301.
- 787 Strom, K., Papanicolaou, A., Evangelopoulos, N., & Odeh, M. (2004). Microforms in gravel bed rivers:
- Formation, disintegration, and effects on bedload transport. *Journal of Hydraulic Engineering*, 130(6),
- 789 554-567.
- 790 Vázquez-Tarrío, D., Piqué, G., Vericat, D., & Batalla, R. (2021). The active layer in gravel-bed rivers: An
- 791 empirical appraisal. Earth Surface Processes and Landforms, 46(2), 323-343.
- Venugopal, V., Roux, S. G., Foufoula-Georgiou, E., & Arneodo, A. (2006). Revisiting multifractality of high-
- 793 resolution temporal rainfall using a wavelet-based formalism. Water Resources Research, 42(6),
- 794 W06D14.

- Viparelli, E., Sequeiros, O. E., Cantelli, A., Wilcock, P. R., & Parker, G. (2010). River morphodynamics with
- 796 creation/consumption of grain size stratigraphy 2: numerical model. *Journal of Hydraulic Research*,
- *48*(6), 727-741.
- 798 Viparelli, E., Balkus, A., Vázquez Tarrío, D., Hill, K. M., Tal, M., & Fedele, J. (2022). Streamwise and
- vertical dispersal of tracer stones in an equilibrium bed. Water Resources Research, 58(11),
- e2022WR033137.
- Voepel, H., Schumer, R., & Hassan, M. A. (2013). Sediment residence time distributions: Theory and
- application from bed elevation measurements. Journal of Geophysical Research: Earth Surface, 118(4),
- 803 2557-2567.
- Wong, M., & Parker, G. (2006). One-dimensional modeling of bed evolution in a gravel bed river subject to a
- 805 cycled flood hydrograph. *Journal of Geophysical Research: Earth Surface*, 111(F3), F03018.
- Wong, M., Parker, G., DeVries, P., Brown, T. M., & Burges, S. J. (2007). Experiments on dispersion of tracer
- stones under lower-regime plane-bed equilibrium bed load transport. Water Resources Research, 43(3),
- 808 W034403.
- 809 Wu, Z., & Chen, G. Q. (2014). Approach to transverse uniformity of concentration distribution of a solute in a
- solvent flowing along a straight pipe. *Journal of Fluid Mechanics*, 740, 196-213.
- 811 Wu, Z., Furbish, D., & Foufoula-Georgiou, E. (2020). Generalization of hop distance-time scaling and particle
- 812 velocity distributions via a two-regime formalism of bedload particle motions. Water Resources
- 813 *Research*, 56, e2019WR025116.
- 814 Wu, Z., Singh, A., Fu, X., & Wang, G. (2019a). Transient anomalous diffusion and advective slowdown of
- bedload tracers by particle burial and exhumation. *Water Resources Research*, 55, 7964-7982.
- 816 Wu, Z., Jiang, W., Zeng, L., & Fu, X. (2023). Theoretical analysis for bedload particle deposition and hop
- statistics. *Journal of Fluid Mechanics*, 954, A11.
- 818 Wu, Z., Foufoula-Georgiou, E., Parker, G., Singh, A., Fu, X., & Wang, G. (2019b). Analytical solution for
- anomalous diffusion of bedload tracers gradually undergoing burial. *Journal of Geophysical Research*:
- 820 Earth Surface, 124(1), 21-37.
- Wu, Z., Singh, A., Foufoula-Georgiou, E., Guala, M., Fu, X., & Wang, G. (2021). A velocity-variation-based
- formulation for bedload particle hops in rivers. *Journal of Fluid Mechanics*, 912, A33.
- Yarnell, S. M., Mount, J. F., & Larsen, E. W. (2006). The influence of relative sediment supply on riverine
- habitat heterogeneity. *Geomorphology*, 80(3-4), 310-324.

825	Zhan, J., Jiang, W., & Wu, Z. (2024). Reactive transport in open-channel flows with bed adsorption and
826	desorption. Journal of Hydrology, 632, 130855.
827	Zhang, Y., Cheng, J., Hassan, M., Wang, P., & Wu, Z. (2024). Drag coefficient of emergent vegetation in a
828	shallow nonuniform flow over a mobile sand bed. Water Resources Research, 60, e2023WR036535.
829	

Figure	1.
--------	----



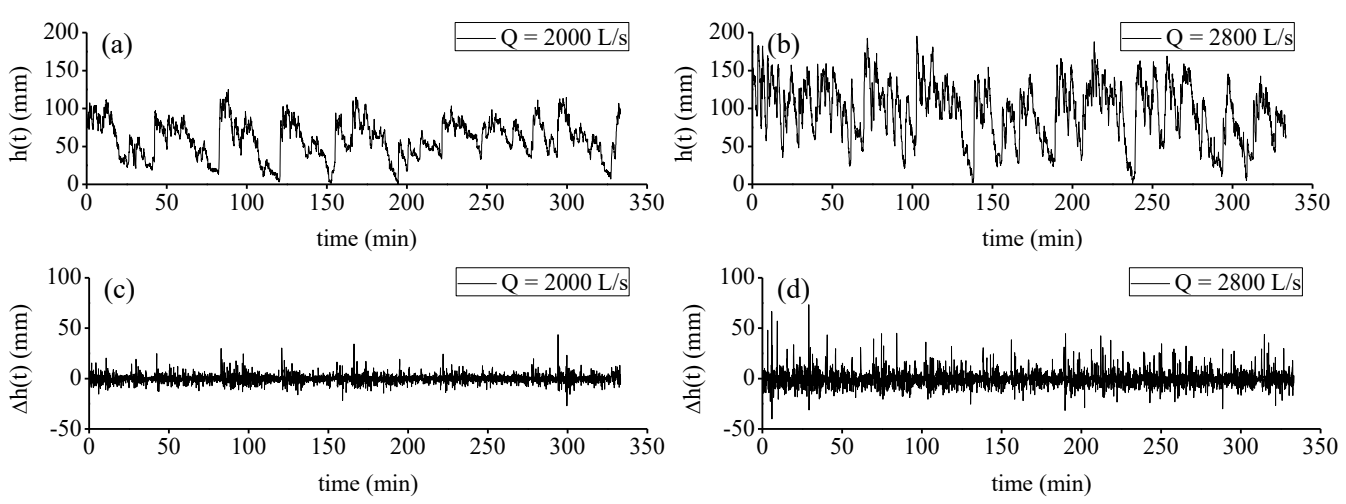


Figure	3.
--------	----

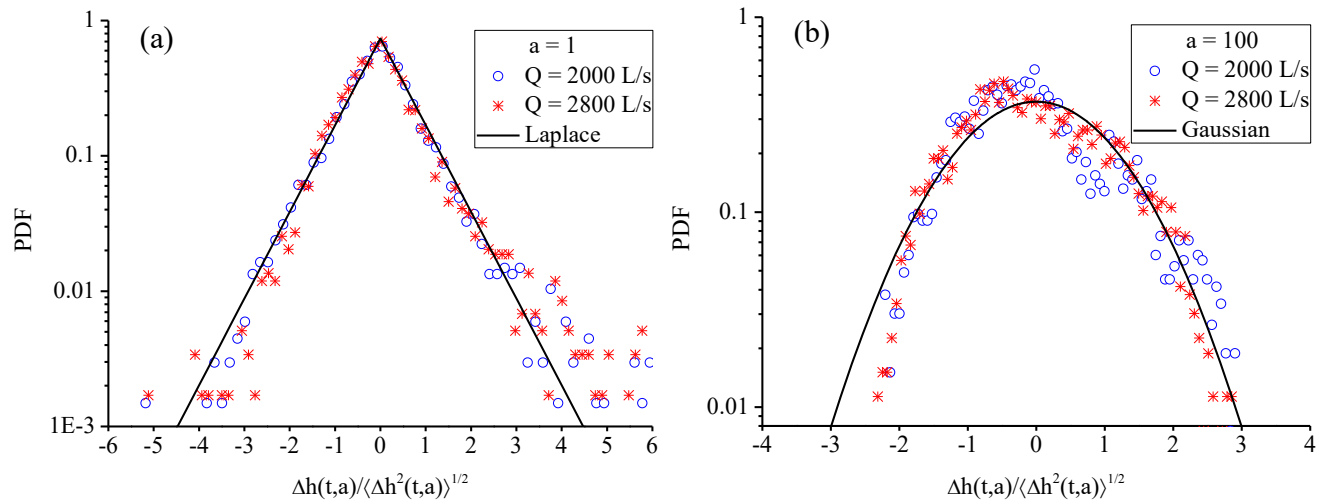


Figure 4.	
-----------	--

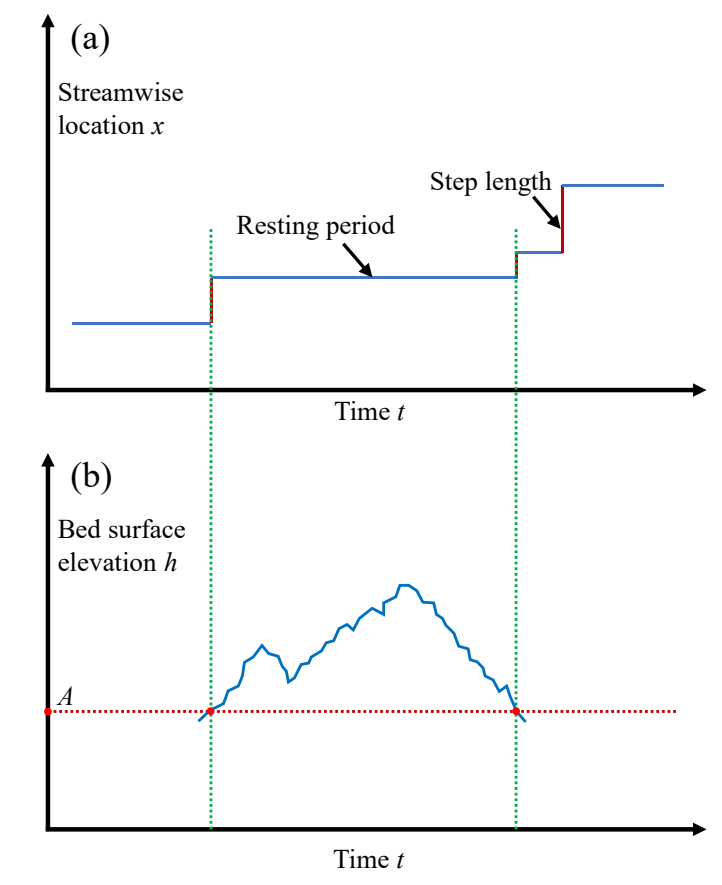
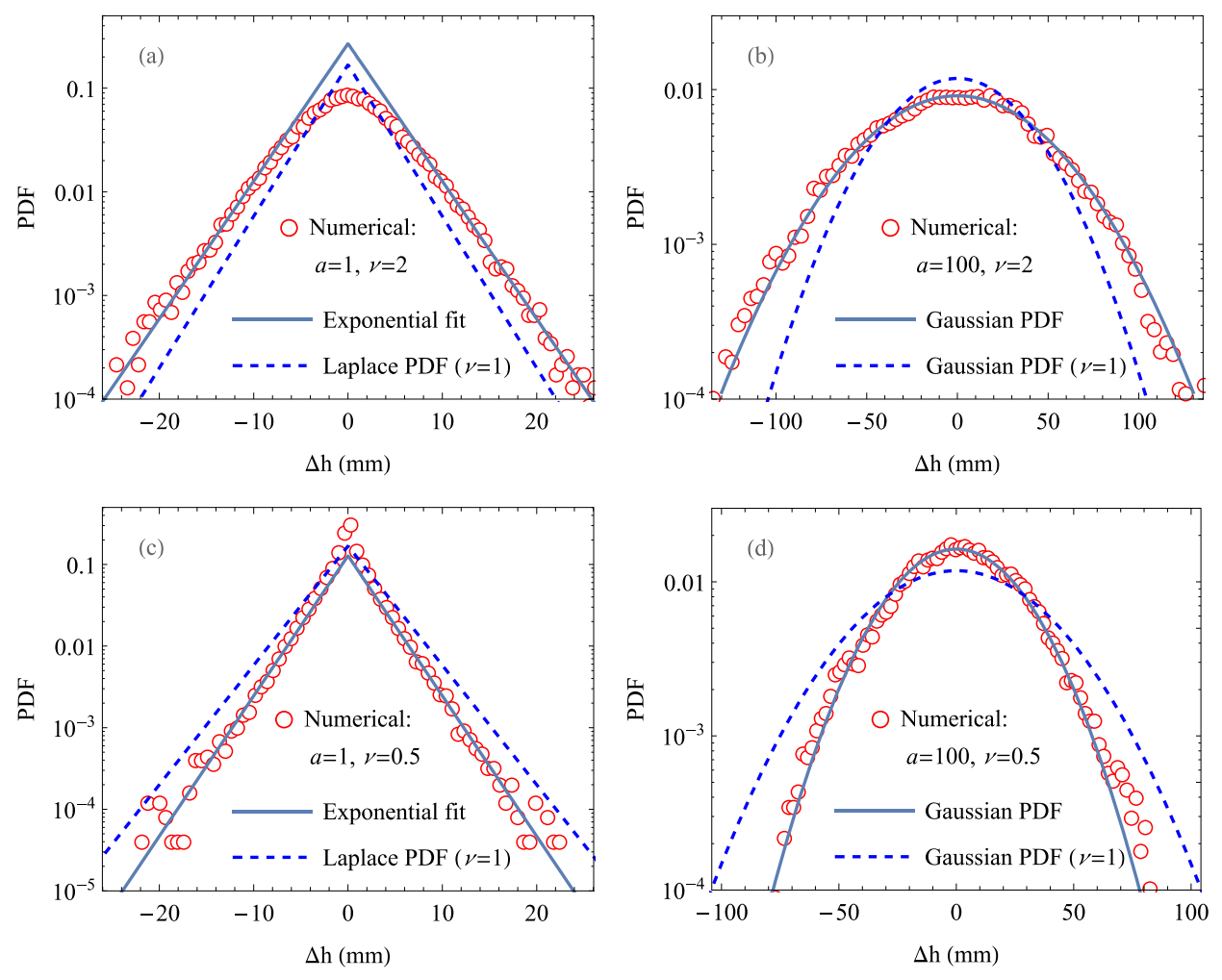


Figure 5.	
-----------	--



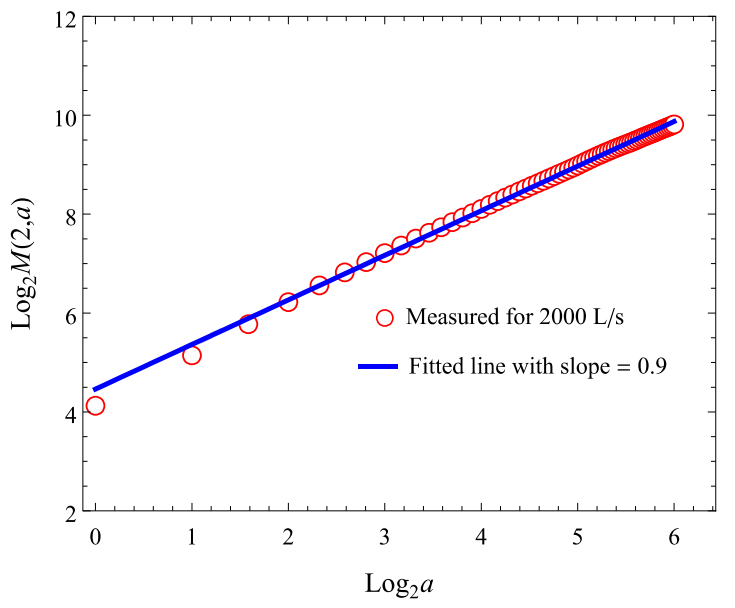


Figure	7	•
--------	---	---

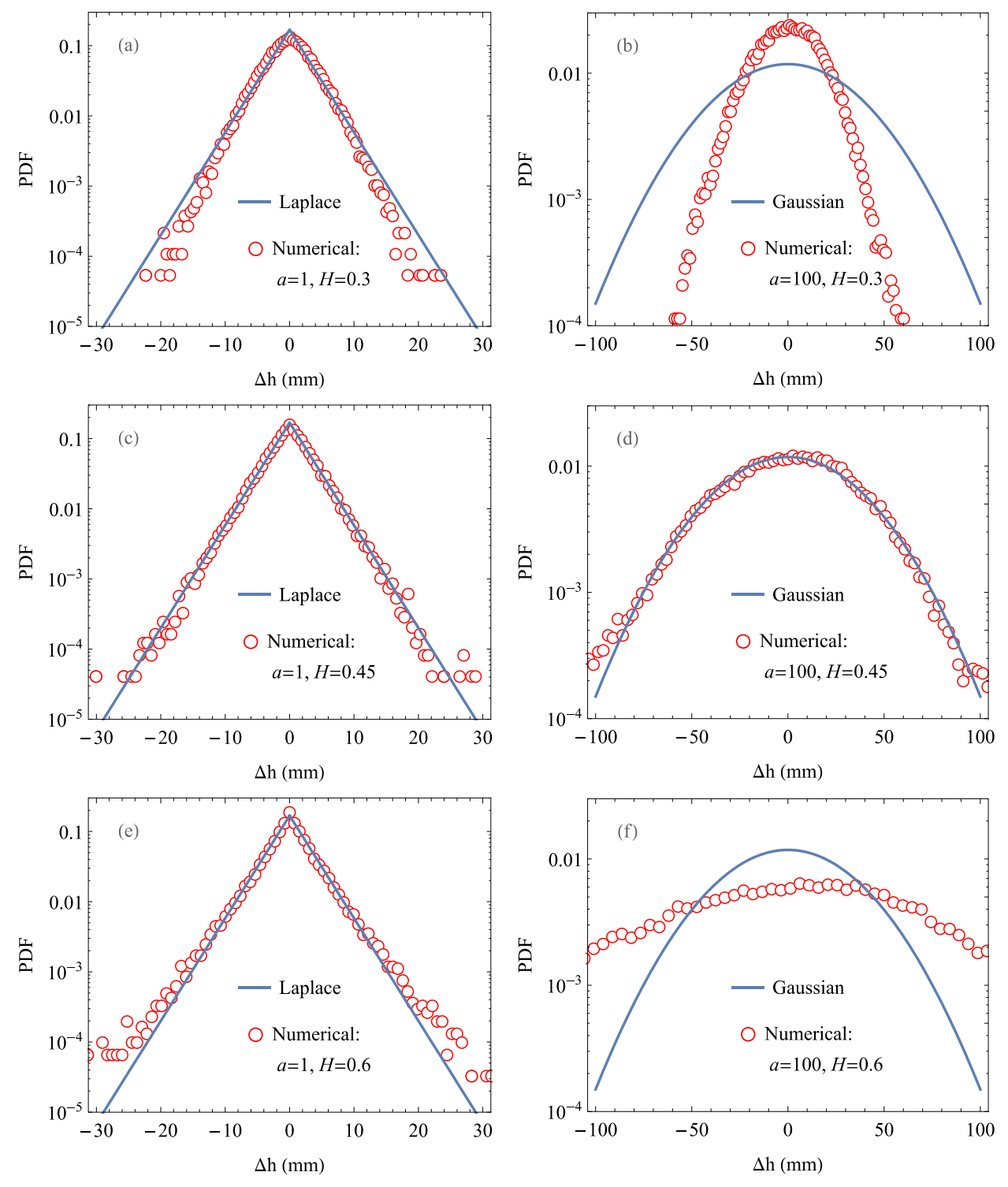


Figure	8.
--------	----

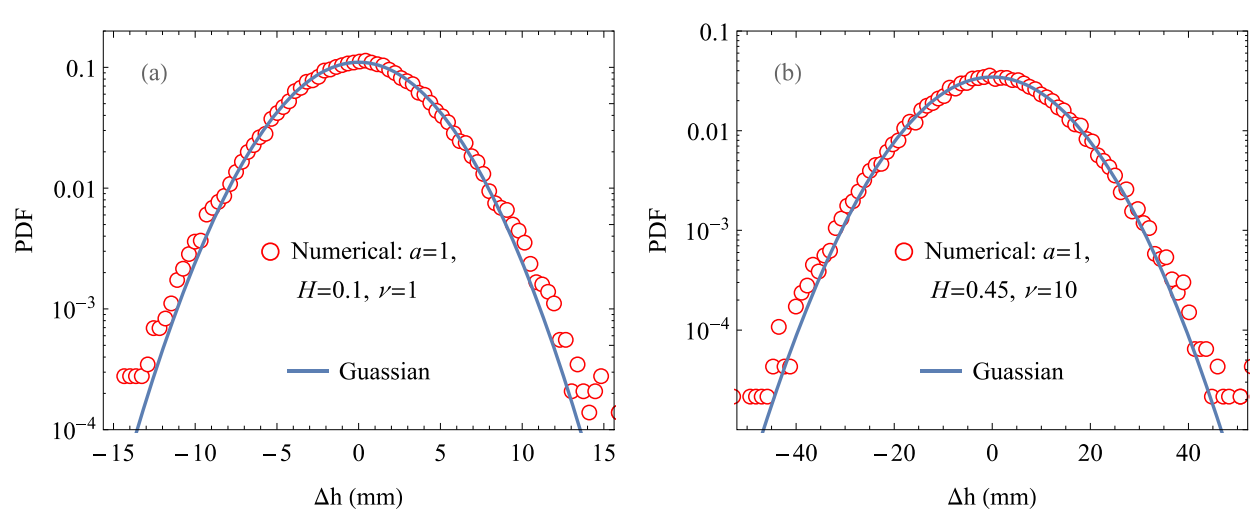


Figure 9.	
-----------	--

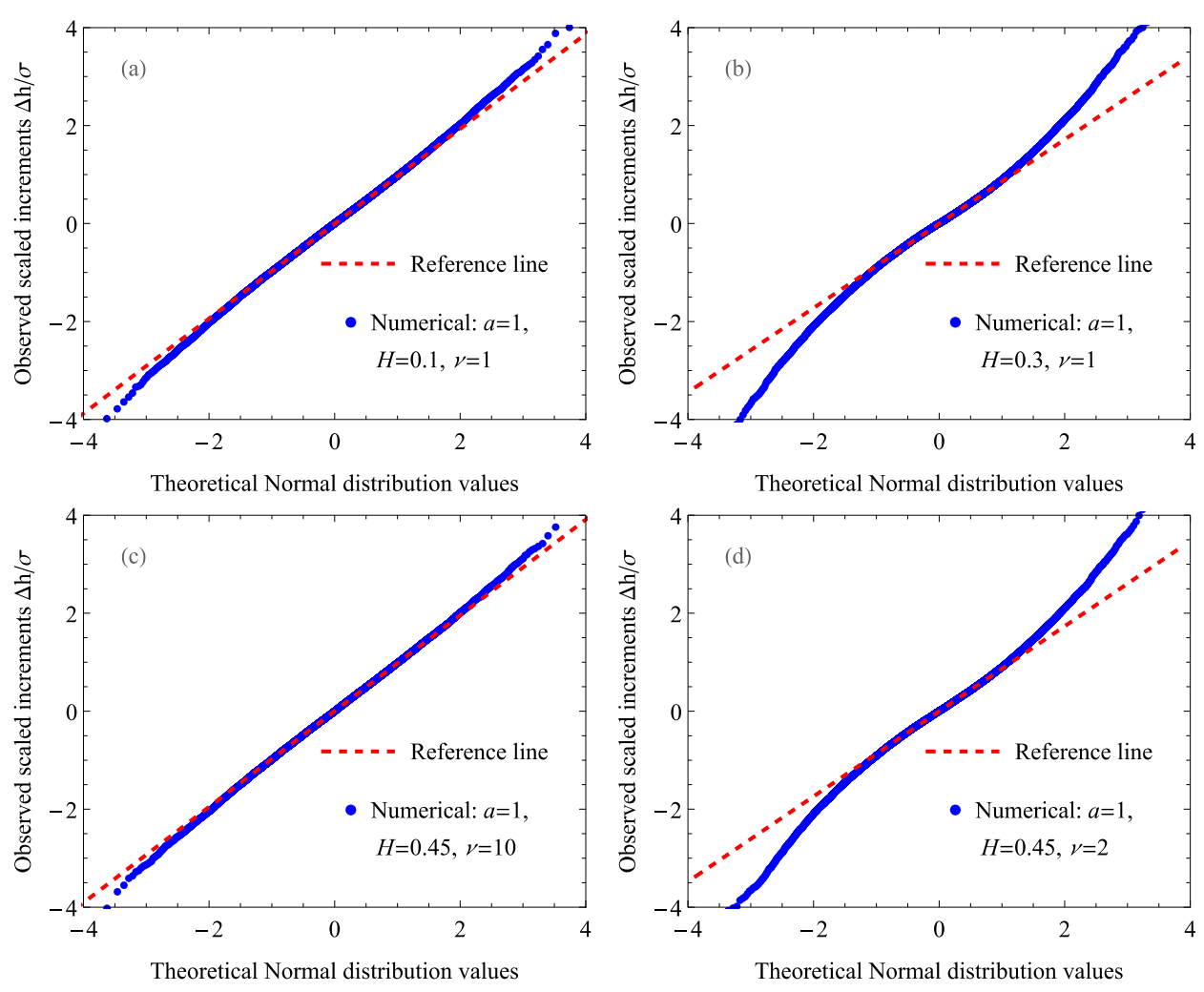
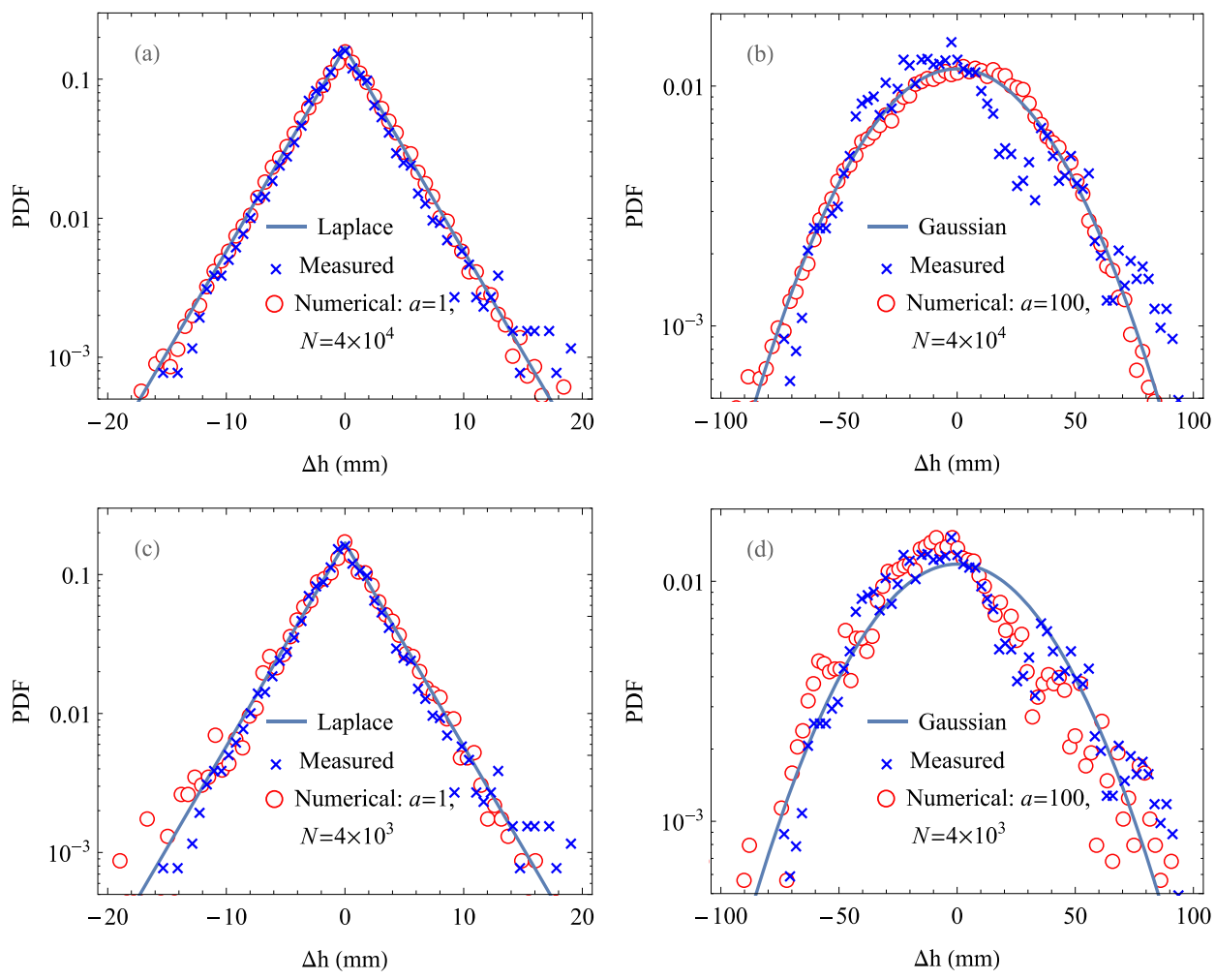


Figure	10.
--------	-----



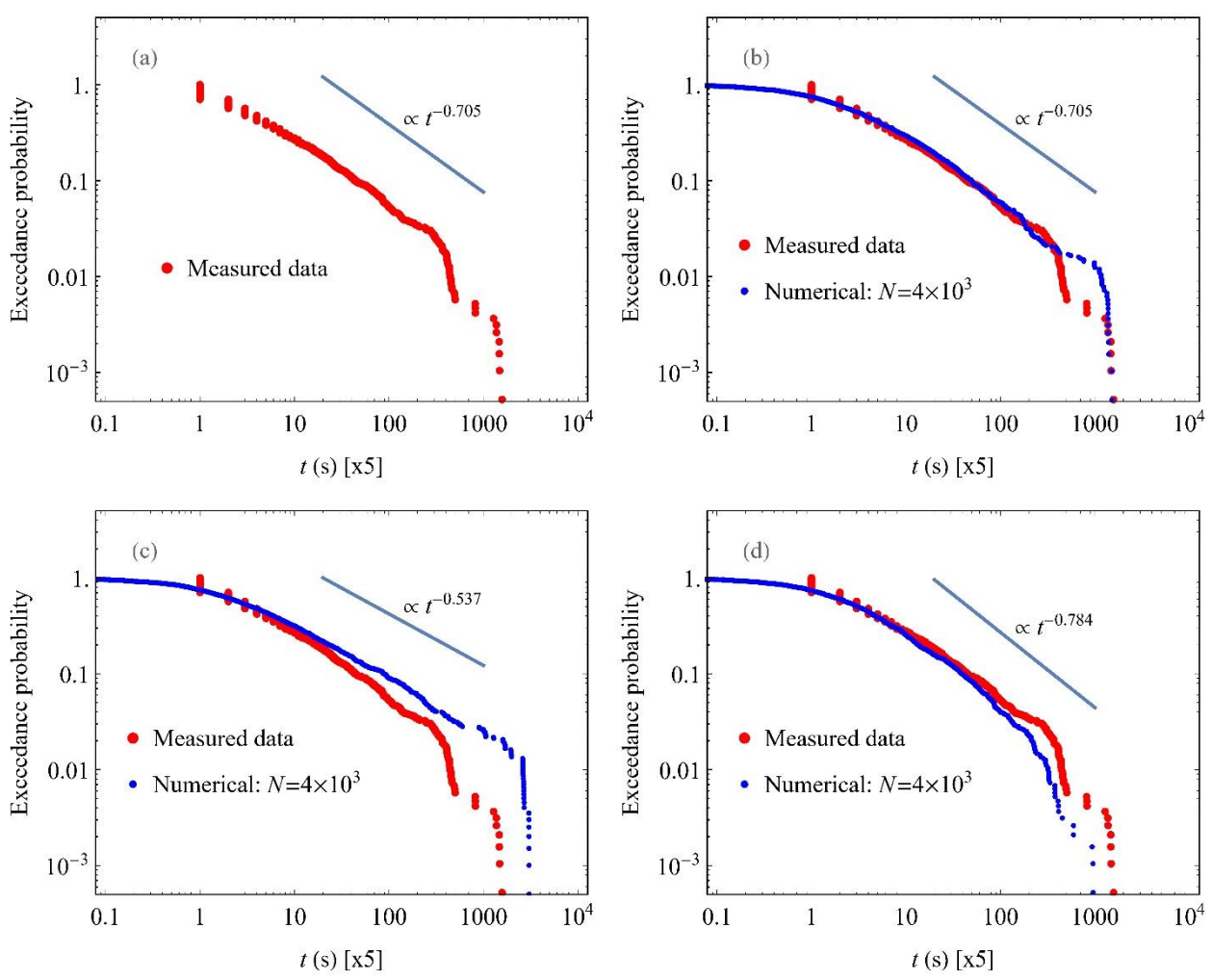


Figure 12	2.
-----------	----

